



Chair of Materials Physics

Master's Thesis

Nanoindentation response of single crystal
copper films on sapphire

Julia Magdalena Sträußnigg, BSc

November 2019



EIDESSTATTLICHE ERKLÄRUNG

Ich erkläre an Eides statt, dass ich diese Arbeit selbständig verfasst, andere als die angegebenen Quellen und Hilfsmittel nicht benutzt, und mich auch sonst keiner unerlaubten Hilfsmittel bedient habe.

Ich erkläre, dass ich die Richtlinien des Senats der Montanuniversität Leoben zu "Gute wissenschaftliche Praxis" gelesen, verstanden und befolgt habe.

Weiters erkläre ich, dass die elektronische und gedruckte Version der eingereichten wissenschaftlichen Abschlussarbeit formal und inhaltlich identisch sind.

Datum 28.10.2019

Julia Sträußnigg

Unterschrift Verfasser/in
Julia Magdalena, Sträußnigg

Acknowledgements

The thesis at hand could not have been accomplished without the help and support of many people.

First, I would like to cordially thank my supervisor Priv.-Doz. Dr. Megan J. Cordill for her extraordinary mentoring and excellent support throughout the development of this thesis. She readily guided me through the experimental part, gave me proper advice how to handle the data analysis and thoroughly corrected the written formation of my thesis. My gratitude for her dedicated supervision and admiration for her scientific ambition are sincere and genuine.

Furthermore, my thank and gratitude belongs to Dr. Gunther Richter for the fabrication and preparation of the samples investigated in this thesis. Without his accurate work this thesis could not have been accomplished.

A very special thank belongs to my family and friends, who provided me with the best mental support, encouraged me to go on when I felt disappointed and never grew tired to praise the light at the end of the tunnel that was about to come.

Contents

1	Abstract	1
2	Introduction	3
3	Theory	7
3.1	Nanoindentation Mechanics	8
3.1.1	Hertzian Theory	8
3.1.2	Hardness	9
3.1.3	Load-Displacement Curves and Elastic Modulus . . .	13
3.1.4	Measurement Errors	17
4	Experimental Procedure	20
4.1	Samples	20
4.2	Indentation experiments	20
5	Results	25
5.1	Bulk Cu and sapphire indents	25
5.1.1	Bulk Cu indents	25
5.1.2	Sapphire indents	28
5.1.3	Summary	31
5.2	Thin film measurements	32
5.2.1	Tip effects	32
5.2.2	Film Thickness Effects	47
5.2.3	Summary	51
5.3	Pop-in analysis	52
6	Discussion	56
6.1	Effect of Pile-up	56
6.2	Determination of reduced elastic modulus from pop-in data	58
6.3	Plastic and Elastic Zones	61
7	Conclusions	65

1 Abstract

Thin films fulfil very significant roles in today's engineering applications. It is of importance to properly determine the mechanical properties to further utilise thin films in an efficient way. The most widely used tool for characterising thin films is nanoindentation, which is mainly applied to extract the hardness and elastic modulus of thin films on substrates. Since 1992, the standard procedure is the Oliver-Pharr method, which is proven to provide correct results for bulk materials, however, it is not sufficient to be applied for the testing of thin films. Although there is common agreement that mechanical properties can be suitably estimated as long as the penetration stays below 10 % of the film thickness, there are many studies that state the problem of obtaining correct values, even below 10 %. Thus, there is a need to investigate this disagreement. This thesis is concentrated on nanoindentation testing of single crystalline (111) Cu films on a single crystalline (0001) sapphire substrate. The material response with respect to tip size, film thickness and indentation load shall be examined. Furthermore, it shall be observed if hardness and elastic modulus provide correct values and if the measured data can be corrected to obtain suitable results. It will be shown that the validity of the 10 % rule of thumb is only appropriate for hardness and elastic modulus cannot be measured for thin films less than 300 nm thick.

Dünne Schichten haben eine entscheidende Rolle in den heutigen technischen Anwendungen inne. Es ist daher notwendig die mechanischen Eigenschaften von Dünnschichten eindeutig zu bestimmen, um sie weiterhin effizient einsetzen zu können. Nanoindentation ist die verbreitetste Instrumentierung, um Dünnschichten zu charakterisieren und wird hauptsächlich für die Bestimmung von Härte und E-Modul verwendet. Die Methode nach Oliver und Pharr wird seit 1992 als Standard zur Ermittlung ebener anerkannt. Sie liefert korrekte Werte für unbeschichtete Grundmaterialien, weist allerdings gravierende Schwächen bei der Untersuchung

von dünnen Schichten auf Substraten auf. Der weit verbreiteten "10%-Regel", also die Bestimmung korrekter Werte solange die Indentierungstiefe 10 % der Schichtdicke nicht überschreitet, wird weitestgehend Gültigkeit zugesprochen. Viele Studien bezweifeln allerdings deren Richtigkeit, da die "10%-Regel" keine verlässlichen Resultate liefert und somit hinterfragt werden muss. Diese Arbeit konzentriert sich auf die Nanoindentierung von einkristallinen (111) Cu Schichten auf einkristallinem (0001) Al_2O_3 -Substrat. Die Materialantwort wird in Abhängigkeit des Spitzenradius des Indenters, der Schichtdicke und der auferlegten Last bestimmt. Darüber hinaus werden die Härte und der E-Modul gemessen, deren Resultate werden überprüft und Korrekturen angebracht, um zu sehen, ob sich dadurch korrekte Werte ergeben. Es wird gezeigt, dass die "10%-Regel" nur für die Härtebestimmung verwendet werden darf und dass der E-Modul für dünne Schichten mit einer Schichtdicke kleiner als 300 nm nicht bestimmt werden kann.

2 Introduction

The goal of many industries is to enhance the performance and reliability of their devices. To achieve this, in many cases thin films are applied on technical components. They are most commonly used in optical or electronic devices and for the purpose of surface refinement. For instance, thin films help to regulate the reflexion behaviour, improve corrosion and wear resistance or adjust the desired electrical functionality. Commonly used materials are oxides, organics and metals such as copper, gold or aluminum. Thin films are usually fabricated using chemical (CVD) or physical vapour deposition (PVD), where the respective material is either deposited via chemical reactions or condensates from the vapour phase. The thickness of thin films ranges from a few nanometers up to several micrometers depending on the manufacturing method and the elastic mismatch between the substrate and the coating material. Usually the hardness and yield stress, σ_{ys} , of thin films can largely deviate from their bulk counterparts, whereas the elastic modulus should stay the same. Due to this circumstance it is crucial to properly investigate the mechanical properties of thin films. The most advantageous and widely used tool to test the mechanical behaviour of thin films is nanoindentation [1] [2] [3].

Nanoindentation, also termed instrumented indentation, is similar to traditional macro hardness testing (e.g. Brinell, Vickers) but designed for much smaller loads and penetrations. It is usually used for extracting mechanical properties, mostly the elastic modulus, E , and hardness, H , from the tested specimens. The standard data analysis procedure is the Oliver and Pharr method [4], which is proven to perform well for the investigation of bulk materials [5]. It is also most frequently used for the testing of thin films, however, it isn't able to account for any effects induced by the substrate [6]. Mainly the deformation of the thin film is constrained by the less deformable substrate during indentation in the case for soft coatings on hard substrates. Thus, the plastic zone, which forms beneath the indenter cannot be fully built and as a consequence the evaluation of elastic modulus and hardness

is interfered [6].

Moreover, there are other artifacts occurring during nanoindentation testing. As such, the indentation size effect (ISE) is experienced as an increase in hardness at decreasing penetration depths below 10 to 20 nm. Nix and Gao [7] explained its appearance in crystalline materials using the concept of geometrically necessary dislocations created during indenting to support the displacement in bulk materials. However, their research requires indentation depths of 3 - 5 μm , which is impractical for the testing of thin films or ultra-thin coatings since their thickness range is much lower. Considering the microstructure of the investigated material and the tip size hardness values may be influenced according to the grain size. Other than that, the determination of hardness is inaccurate when the material of the sample in question is pressed upwards adjacent to the indenter. This case is called pile-up and leads to an overestimation of hardness [6]. The opposite happens when the material around the indenter flows down- and inwards, which is referred to as sink-in. For indenting coated materials it is common to apply the so-called "10 % rule of thumb", meaning that the indenter is not to penetrate the coating more than 10 % of its thickness to obtain a hardness value for the coating, as shown in Fig. 1.

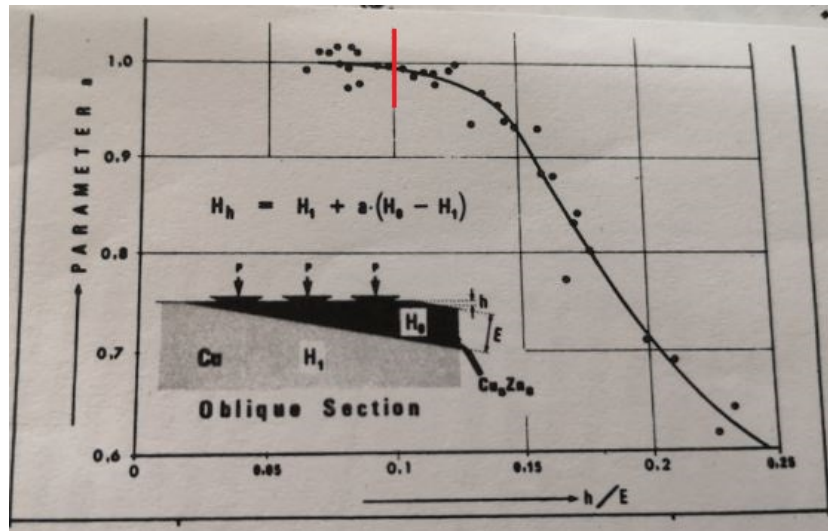


Figure 1: Original proclamation of the 10 % rule of thumb. The parameter s represents hardness and E in this case refers to the film thickness. The 10 % rule of thumb stems from the condition that hardness starts to drop at $\frac{h}{E}=0.1$ and is confirmed for film thicknesses between 5 and 50 μm [8].

This concept was first stated by Bückle [8] in 1973 and originally refers to the investigation of hard coatings on softer substrates only. The system in Fig. 1 is composed of a Cu_5Zn_8 thin film and a CuZn substrate. Hardness tests were carried out using microindentation and the 10 % rule of thumb is indicated by a drop in hardness from $\frac{h}{E}=0.1$ onwards and was confirmed for thicknesses between 5 and 50 μm [8], with E being the film thickness in this case. Although this rule is for hardness measurements only, it is consistently used for the evaluation of the elastic modulus of thin films as well [9] [10] [11] [12].

The indentation community has ignored the original work and assumed that since hardness is measured from plastic deformation, and the elastic modulus from elastic behaviour, could be treated the same for thin films. This assumption is wrong when the original definition is consulted because microindents were utilized which can only produce a measurement of hardness.

The focus of this thesis is on how soft films on hard substrates deform under indentation loading. It shall be demonstrated that the 10 % rule of thumb is not suitable for the extraction of elastic modulus, however, hardness can be sufficiently determined for larger displacement ranges, namely beyond the 10 % restriction depending on the respective thin film and substrate system. Furthermore, the mechanical response with respect to different tip sizes and film thicknesses of single crystalline Cu films on sapphire is investigated. The results obtained for films on substrates are compared to values of the respective bulk materials.

3 Theory

Nanoindentation, also termed instrumented indentation, is similar to traditional macro hardness testing (e.g. Brinell, Vickers) but designed for much smaller loads and penetrations. In order to perform an indent a hard tip, usually made of diamond, is pressed into contact with the material. During the indentation process the load as well as the penetration depth are measured continuously. When the contact force has reached its test maximum it decreases and the displacement recovers elastically, leaving an imprint caused by plastic deformation. A schematic representation is depicted in Fig. 2.

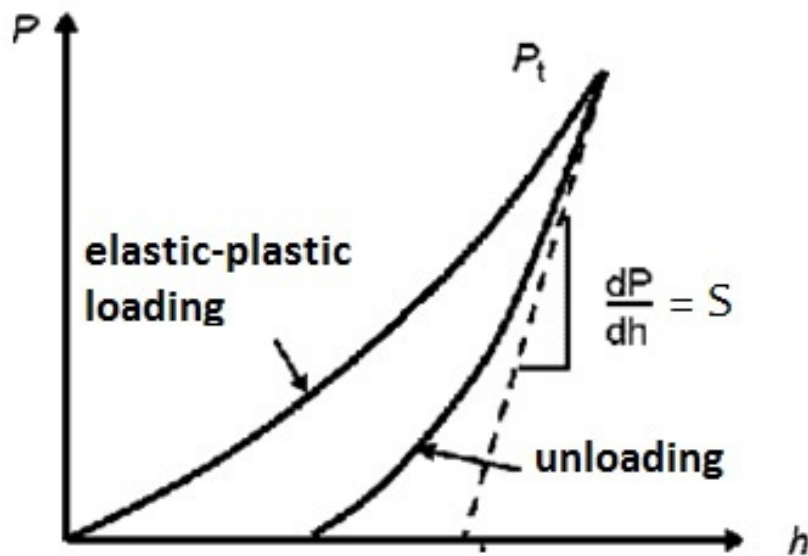


Figure 2: Schematic load-displacement curve for data analysis [13].

Nanoindentation is most commonly used to determine the hardness and elastic modulus of a material and is also well suited to investigate small volumes of thin films on substrates [13]. Moreover, it can also be used for adhesion testing [14] and also to investigate the fracture behaviour of materials [15].

3.1 Nanoindentation Mechanics

3.1.1 Hertzian Theory

In general nanoindentation works like conventional hardness testing, however, the loads applied are in the range of μN (10^{-6} N) to mN (10^{-3} N) and the achieved penetration depths have a resolution of nanometres (10^{-9} m). Hence, these small ranges hold several challenges when it comes to extracting mechanical properties from the investigated specimen. For nanoindentation experiments this means obtaining values for the elastic modulus, E , and hardness, H , of the sample.

In order to measure the above mentioned material properties the process when two solids, the indenter and the specimen surface, are pressed into contact must be observed. Hertz [16] considered the purely elastic case for a spherical rigid indenter and a flat sample surface, depicted in Fig. 3. The relation between the radius of contact, a , indenter load, P , and indenter radius, R , is given by

$$a^3 = \frac{3}{4} \cdot \frac{P * R}{E^*} \quad (1)$$

whereas E^* is referred to as the combined or reduced modulus, a combination of the elastic properties of both indenter and specimen. It can be interpreted as

$$\frac{1}{E^*} = \frac{(1 - \nu_1^2)}{E_1} + \frac{(1 - \nu_2^2)}{E_2} \quad (2)$$

with E_1 and ν_1 being the modulus and Poisson's ratio of the sample and E_2 and ν_2 of the indenter.

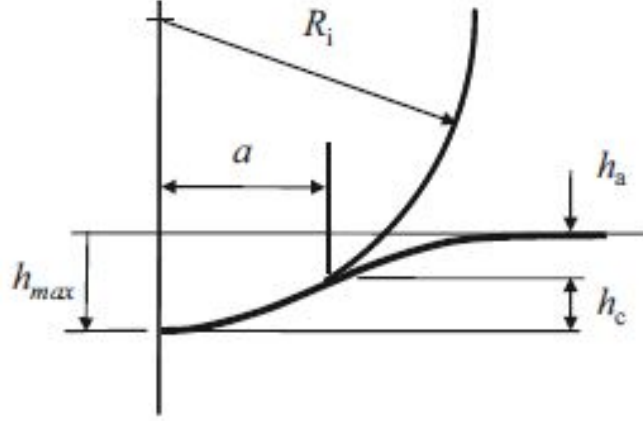


Figure 3: Contact between a spherical indenter and a flat surface. R_i is the radius of the indenter and a represents the contact radius. The total displacement depth, h_{max} , is divided into the depth from the edge of the circle of contact, h_c , and the depth from the surface to the circle of contact, h_a [16].

Taking into account the total displacement beneath the specimen surface, h_t , when the maximum load is applied on the indenter and combining it with Eqn. (1) and Eqn. (2) it yields

$$P = \frac{4}{3}E^*R^{\frac{1}{2}}h_t^{\frac{3}{2}} \quad (3)$$

giving a relation between the applied load, P , and the displacement, h , including the reduced elastic modulus, E^* , and tip radius, R .

3.1.2 Hardness

Elastic deformation between two solids, as discussed in section 3.1.1 leaves no permanent imprint. Hardness is generally explained as a material's resistance against plastic deformation caused by another harder material. Plastic deformation and the resulting residual impression with area, A , is necessary to make assumptions about a material's hardness using the common relation

$$H = \frac{P}{A} \quad (4)$$

with P representing the load. In nanoindentation experiments the mean contact pressure p_m , which is given by the indenter load P divided by the contact area A , is taken as an equivalence for hardness. As nanoindentation applies the projected or contact area as a measure for hardness, the latter and the mean contact pressure are directly related.

Macro hardness testing uses optical tools to measure the area for calculating hardness. However, for nanoindentation experiments the applied loads and resulting indents scale on much smaller dimensions. This makes a valid evaluation of the correct area almost impossible. In order to solve this problem geometrical relations are taken advantage of namely calibration of the tip with an area function.

It should be shortly mentioned that there is a wide variety concerning different shapes of indenters. The most prominent ones are the spherical indenter, which has the shape of a sphere, the conical indenter, which has a pointed end, the Vickers and the Berkovich indenter. A Vickers tip has the shape of a four-sided pyramid and the Berkovich tip has the form of a three-sided pyramid. For several reasons Berkovich is the most ideal tip to be used. Amongst other advantages it is not easily damaged and relatively easy to be manufactured [13]. In this thesis only the Berkovich tip was used. Fig. 4 provides an overview of the different indenter types.

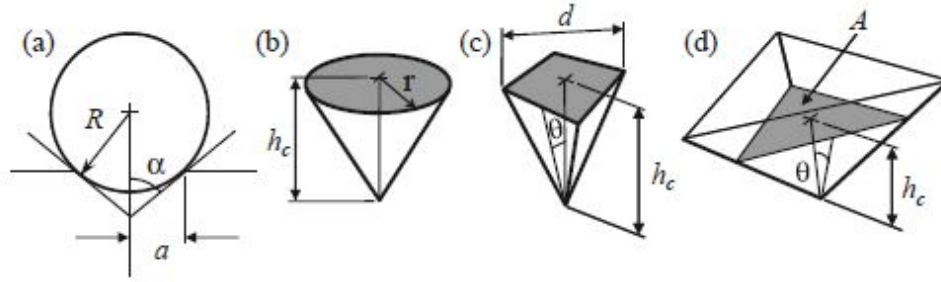


Figure 4: a.) spherical indenter b.) conical indenter c.) Vickers indenter d.) Berkovich indenter [16]

Nanoindentation is referred to as depth-sensing indentation, whereby the displacement of the indenter beneath the surface is continuously measured. The displacement from the edge of the circle of contact, h_c or the contact depth (see Fig. 3), is significant in determining the contact area, A , of the indenter tip in use. The contact area is a function of contact depth $A = f(h_c)$, whereby the exact form of this function is termed area function [13]. For the Berkovich tip the area function is expressed as:

$$A = 3\sqrt{3}h_c^2 \tan^2 \theta \quad (5)$$

with h_c being the contact depth and θ being the semiangle of the tip faces. Originally θ was fashioned to be 65.03° but was later changed to 65.27° . The first value gives the same ratio of actual area to indentation depth as for the Vickers indenter. θ was changed to the latter value which gives the same ratio of contact area to indentation depth as a Vickers tip. This satisfies the nanoindentation definition of hardness, that is directly connected to the mean contact pressure p_m .

With a fixed θ Eqn. (5) becomes $A = 24.5h_c^2$ and hardness can be calculated as

$$H = \frac{P}{24.5h_c^2} \quad (6)$$

for an ideal Berkovich indenter.

Since indenter tips are not ideally shaped it is required to correct the imperfect tip area in order to obtain correct measurements. This is achieved by repeatedly indenting a material with known reduced elastic modulus, E^* , usually Fused Quartz. For calculating the area function the unloading stiffness, $\frac{dP}{dh}$, is measured and with a known value for E^* the area, A , can be calculated from Eqn. (7). Details about the calculation of E^* from nanoindentation are treated in the following section.

$$E^* = \frac{1}{2} \frac{\sqrt{\pi}}{\sqrt{A}} \frac{dP}{dh} \quad (7)$$

The area, A , is then plotted over the displacement, h , and a polynomial fit is applied. This polynomial fit is necessary to determine the coefficients C_1 , C_2 , ... from Eqn. (8)

$$A(h_c) = C_0 * h_c^2 + C_1 * h_c + C_2 * h_c^{\frac{1}{2}} + C_3 * h_c^{\frac{1}{4}} + C_4 * h_c^{\frac{1}{8}} + \dots + C_8 * h_c^{\frac{1}{128}} \quad (8)$$

in order to obtain a correct area of contact since $C_0=24.5$ is only applicable for an ideal Berkovich tip. The area function is in correct alignment with theory at larger penetration depths (2 μm), however, at lower penetration depths it deviates from the correct form due to blunting of the tip depending mostly on the wear rate [13].

To apply Eqns. (5) and (6) the contact depth must be known. For pyramidal indenters it is equated from

$$h_c = h_t - 0.75 \frac{P}{S} \quad (9)$$

with h_t being the respective indentation depth and S representing the stiffness, a differential $\frac{dP}{dh}$ during unloading, as described in following section 3.1.3.

3.1.3 Load-Displacement Curves and Elastic Modulus

During the indentation process the load, P , as well as the displacement h are measured continuously resulting in a load-displacement curve or compliance curve, which is shown in Fig. 5. The test proceeds as follows: when the indenter is in contact with the sample surface a force is applied, that increases from zero towards a maximum load, P_{max} . This part is termed elastic-plastic loading, where the material deforms accordingly. Upon reaching P_{max} the maximum displacement, h_{max} , is obtained. This marks the end of the loading cycle and is followed by unloading, where the load is again reduced to zero. According to the mechanical behaviour of the tested specimen the maximum displacement is divided into two contributions: the elastic displacement, h_e , which is recovered during unloading, and the plastic displacement, h_r , which is permanent and marks the depth of a residual imprint. The unloading stiffness, S , a differential $\frac{dP}{dh}$, is related to purely elastic unloading and its prolongation crosses the abscissa. This crossing point distinguishes between the h_c and h_a , whereas h_c is the depth of the radius of contact and h_a is the depth from the specimen surface to the edge of the radius of contact. The contact depth h_c is the crucial parameter necessary for determining hardness and elastic modulus.

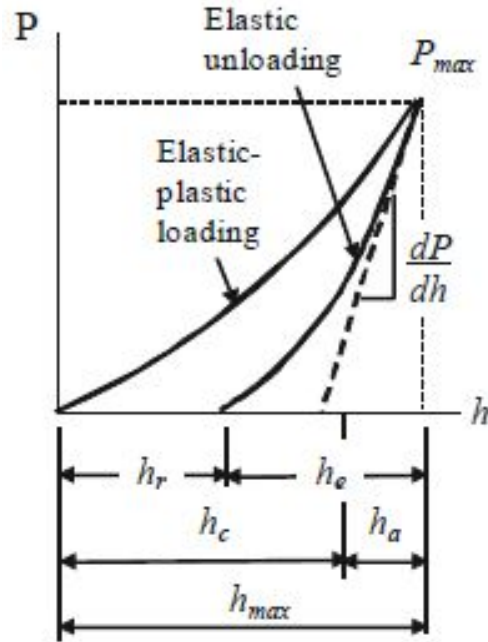


Figure 5: Load-displacement curve with elastic-plastic loading, followed by unloading. The unloading stiffness S , $\frac{dP}{dh}$, is related to purely elastic recovery. The total displacement h_{max} can be divided into h_e , the part of that recovers elastically, h_r , the depth of the permanent imprint, h_c , the depth of the radius of contact and h_a , the depth from the specimen surface to the edge of the radius of contact [16].

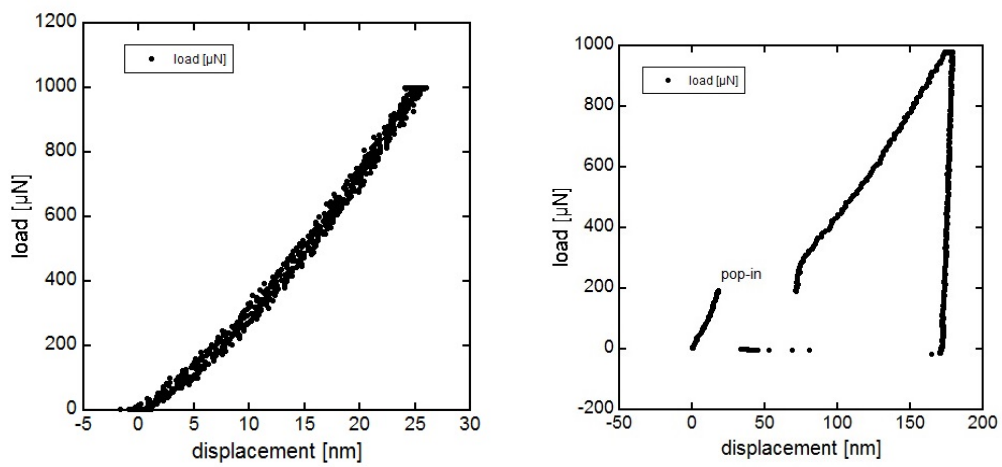
During nanoindentation testing, the reduced elastic modulus, E^* , is determined using following equation

$$E^* = \frac{1}{2} \frac{\sqrt{\pi}}{\sqrt{A}} \frac{dP}{dh} \quad (10)$$

with differential $\frac{dP}{dh}$ representing the unloading stiffness S and A the contact area according to the used indenter shape. With known reduced elastic modulus, E^* , the elastic modulus, E , of the specimen can be calculated from Eqn. (2).

In Fig. 6 and 7 there is an overview about different materials and their corresponding $P-\delta$ curves obtained from the experiments of this thesis with a maximum load of 1000 μN . Sapphire as a brittle material exhibits a large

elastic recovery resulting in a small plastic work of indentation, indicated by the area within the P- δ curve, and a small residual displacement [17]. Cu as a metal demonstrates more plastic deformation, again indicated by the area within the P- δ curve, with a larger residual penetration depth and less elastic recovery. For the case of a single crystal Cu thin film on a sapphire substrate the behaviour is influenced by the respective composite system changes, thus depending on the coating thickness.



(a) Purely elastic indent of sapphire. (b) Plastic indent of Cu with yield excursion.

Figure 6: Typical P- δ curve of sapphire and bulk Cu with a maximum load of 1000 μN .

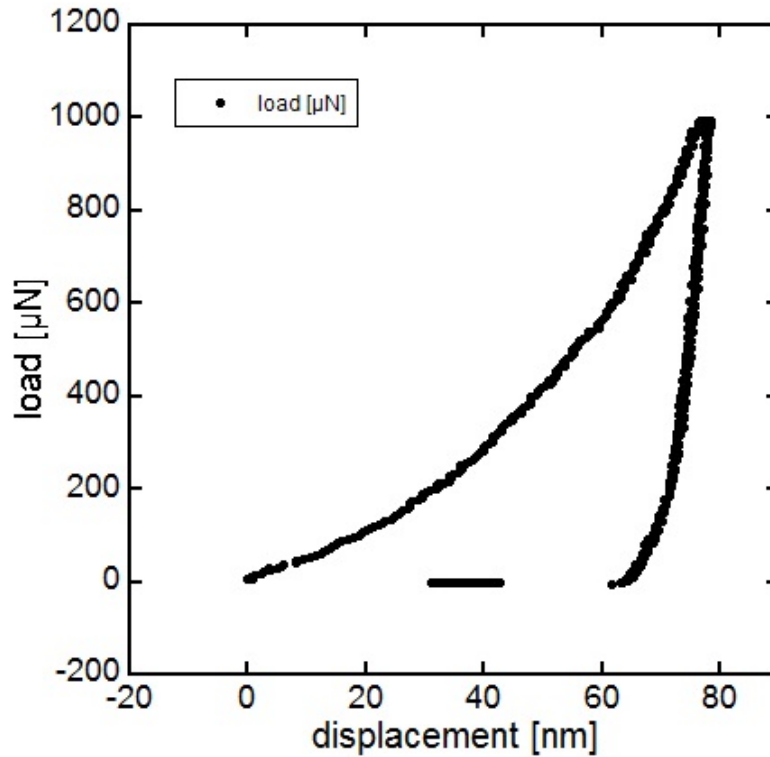


Figure 7: Typical P- δ curve of 100 nm Cu film on sapphire with a maximum load of 1000 μN .

The P- δ curve of Cu in Fig. 6 demonstrates a so-called pop-in event, also referred to as plastic yield excursion [18] [19]. This is characterised by a constant load but continuous change in displacement. At low loads the P- δ curve follows the Hertzian curve of elastic loading until the indenter encounters a defect, such as a dislocation. As a consequence stresses are generated which lead to the activation of many dislocations that are accelerated to near-terminal velocities [20]. Several dislocations are activated and lead to a sudden material flow away from the indenter and are only stopped upon reaching a low enough shear stress, τ_{arrest} [20]. Thus, the load on the indenter remains constant until it is again in contact with the material and can increase further. It is an indicator for the plastic behaviour of materials and can often be related to fracture events or phase changes inside the specimen.

3.1.4 Measurement Errors

There are several errors that can occur during nanoindentation testing that affect the measured data. The issues that feature most prominently are thermal drift, initial penetration depth, frame compliance and piling-up or sinking-in. The measurement errors most commonly influence the displacement recording. Any thermal change during indenting that causes either the sample or the test instruments to thermally expand and affect the displacement reading. In order to correct for such errors the surrounding conditions must be kept constant. Another issue that influences improper displacement reading is the initial penetration depth. For nanoindentation testing it is required that the displacement recording starts when the indenter is in contact with the surface. To fulfill this condition an initial force must be applied to the instrument. This causes a penetration into the material no matter how small the contact force is. To obtain correct results the initial displacement must be added to the total displacement. Furthermore, the deflection of the instrument frame, specimen holder and indenter shaft change linearly with the applied load and have a falsifying effect on the indentation data since the entire displacement, including that of the instrument, is recorded. This compliance is the inverse factor of the unloading stiffness, S , which is required for the calculation of the reduced modulus, E^* . In general, the frame compliance is subtracted from the experimental values before the reduced elastic modulus is evaluated [16].

Material-dependent phenomena that manipulate hardness values are pile-up and sink-in. According to the material specific value E/Y this behaviour leads to either under- or overestimation of hardness, where E again is the elastic modulus of the specimen and Y is the specimen's yield stress. Materials with a low E/Y value, that are materials with no further possibility of hardening (e.g. work hardened) or soft films on hard substrates, pile up whereas specimens with a high E/Y value, e.g. ceramics, sink in [21]. Pile-up signifies that material around the indenter is pushed up- and outwards, thus increasing the projected area and hardness is overestimated.

The opposite happens with sink-in whereby the material is drawn in- and downwards, decreasing the area that supports the plastic deformation and thus underestimating the samples hardness [22]. The reason for this is portrayed in Fig. 8. Although the Oliver-Pharr method accounts for a certain sink-in around the indenter, the actual contact depth h_c changes when pile-up or sink-in occurs [22].

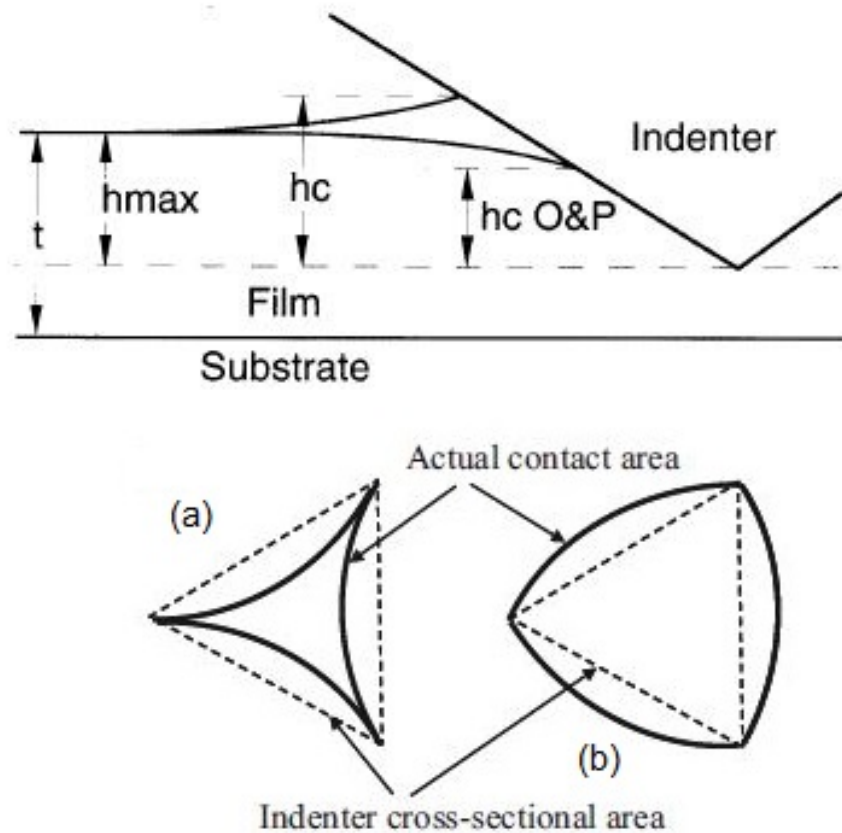


Figure 8: The Oliver-Pharr method assumes h_c O&P to scale linearly with indentation depth, whereas the actual h_c can either be smaller or larger according to a.) sink-in or b.) pile-up and as a consequence hardness is over- or underestimated [16] [22].

In order to correct these errors it is most common to image the indents using AFM (Atomic Force Microscopy) or SPM (Scanning Probe Microscopy) and

then measure the actual area of the imprint using a proper software such as Gwyddion or ImageJ.

4 Experimental Procedure

4.1 Samples

In this thesis three coated specimen and two bulk samples were used. The thin film samples consist of a (0001) sapphire substrate with three different thicknesses of (111) single crystalline Cu thin films. The thickness variation was 300 nm, 100 nm and 50 nm. The bulk materials were Sapphire and single crystalline Cu. The thin films were deposited using Molecular Beam Epitaxy (MBE) by G. Richter in Stuttgart. The lattice of Cu was made to match that of the sapphire substrate in terms of epitaxy. Hence, the atoms in the interface have a coherent or semicoherent transition. This means that no lattice mismatch arises but rather substrate and thin film exhibit almost the same lattice spacing. The condition is graphically depicted in Fig. 9.

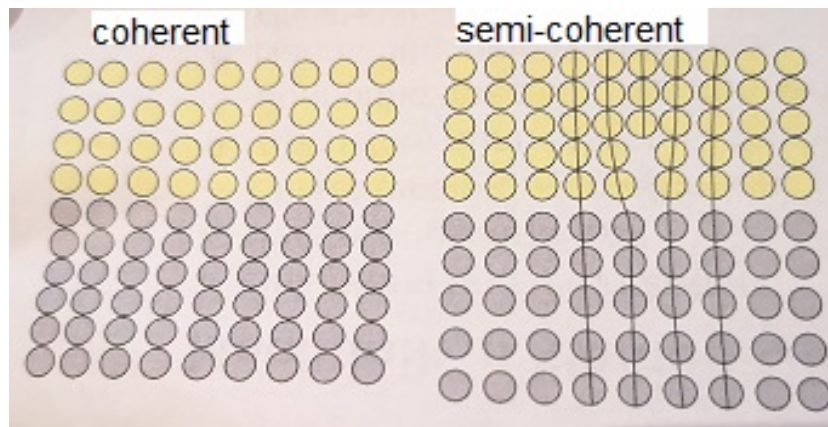


Figure 9: Difference between coherent and incoherent interfaces. The samples in this thesis are fabricated to have a coherent interface.

4.2 Indentation experiments

On each sample a run of indents was performed using two different nanoindentation devices: the Hysitron TriboScope and Hysitron PI 950. The applied force range started with a maximum load of 10 mN and decreasing down to 100 μ N with a spacing of 500 μ N in between. The indents were run in open loop mode. A holding sequence was implemented in the unloading

process to correct for thermal drift. Every other indent was imaged using SPM techniques. For each indent a P- δ curve was produced.

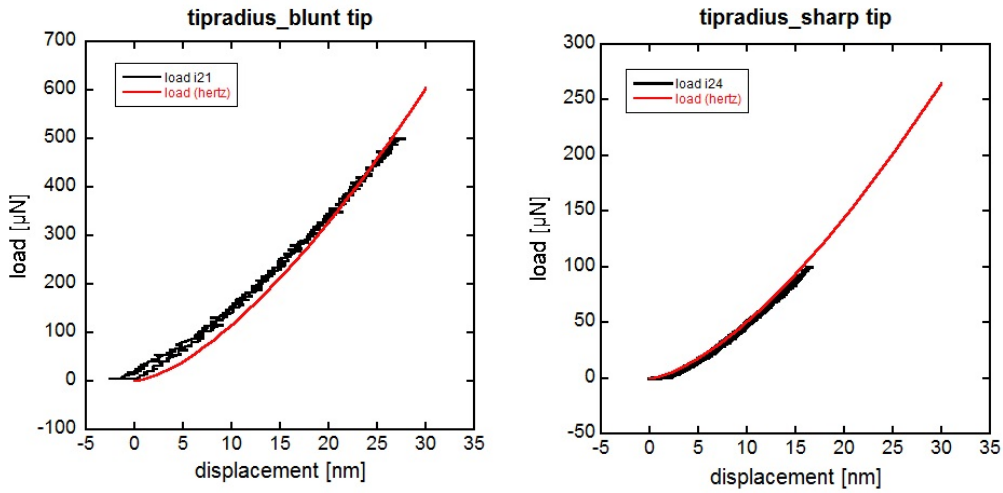
An area function was calculated, as described in section 3.1.2, for each tip by indenting Fused Quartz with a total number of 25 indents each. The tips were then well calibrated using the known reduced modulus of Fused Quartz of 69.9 GPa.

Hardness and elastic modulus were extracted from the experimentals using the Oliver-Pharr method. Both properties were later plotted over $\frac{h_c}{t}$ to indicate a linear scaling factor [5].

In this thesis two different tips were used: a blunt tip and a sharp tip. The radii were calculated using the calibration data of the elastic indents performed in Fused Quartz. With known reduced modulus, E^* , preassumed displacement values, h , the corresponding load, P , for elastic contact was calculated applying Eqn. (11),

$$P = \frac{4}{3} E^* R^{\frac{1}{2}} h_t^{\frac{3}{2}} \quad (11)$$

by varying the tip radius, R . The obtained load was then plotted using KaleidaGraph and seen to match the experimentally obtained data of Fused Quartz. The fit is depicted in Fig. 10 for the blunt tip and the sharp tip the correct radius was found. In this case it was found that the blunt tip radius was 1.6 μm and the sharp tip radius was 300 nm.



(a) Radius calculation for the blunt tip. (b) Radius calculation for the sharp tip.

Figure 10: Suitable fit between the experimental P - δ data and the Hertzian elastic contact to estimate the tip radius.

As explained in section 4.2 the Oliver-Pharr method does not consider pile-up. In order to correct for the piling-up of the Cu and Cu films on sapphire the actual contact area was measured from the SPM images using ImageJ and hardness was obtained from $H = \frac{P}{A}$. The measurement of the actual contact area is depicted in Fig. 11. The height and width of the pile-ups were examined drawing cross-section across each of the indents edges as shown in Fig. 12.

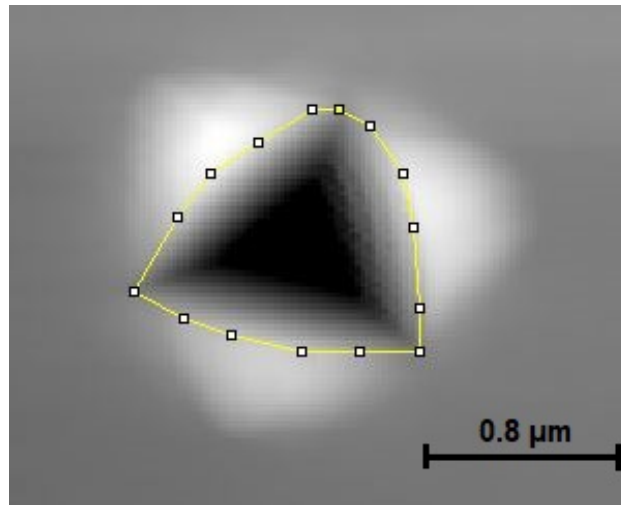
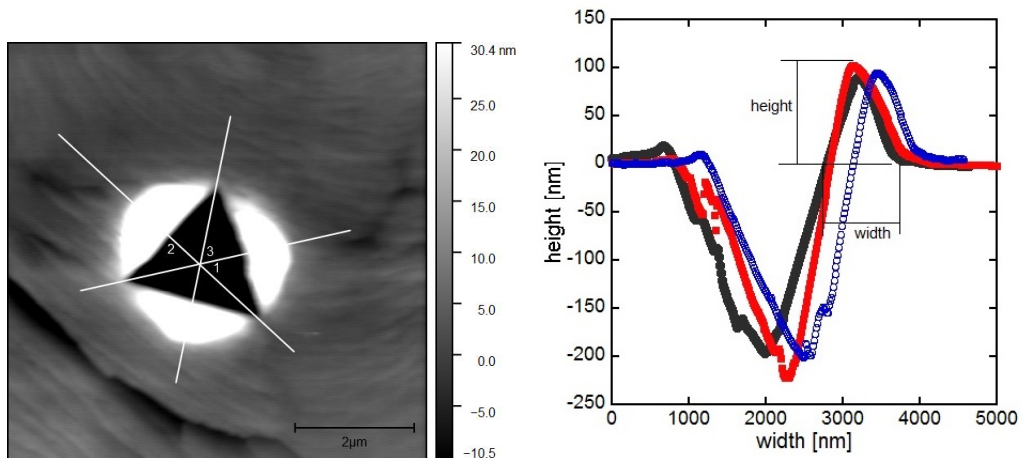


Figure 11: Calculated area of 100 nm Cu film on sapphire using ImageJ.



(a) SPM image of 300 nm Cu film on sapphire with crosssections. (b) Extraction of pile-up height and width.

Figure 12: Data analysis for correction for pile-up.

The bulk Cu and 300 nm sample exhibited an ample amount of pop-ins, which were used to calculate the number of dislocations involved in the geometry of the imprint by dividing the pop-in length by the Burgers vector, b . Furthermore, the stress necessary to obtain pop-ins was examined by calculating τ_{exc} from [18]

$$\tau_{exc} = \frac{P_{exc}}{\pi(2R\delta_i - \delta_i^2)} \quad (12)$$

with P_{exc} and δ_i being the indentation load and displacement at the point where the pop-in starts and R being the indenter radius.

Moreover, the size of the plastic zone beneath the indenter was examined to gain more insight about the hardness measurement of thin films. If the plastic zone radius is lower than the film thickness, useable hardness data should be delivered. The plastic zone radius, c , is schematically depicted in Fig. 13 and is calculated from [23]

$$c = \left[\frac{3P}{2\pi\sigma_{ys}} \right]^{\frac{1}{2}} \quad (13)$$

with P being the indentation load and σ_{ys} the yield stress, calculated from the Tabor relation [24] $\sigma_{ys} = \frac{H}{2.8}$.

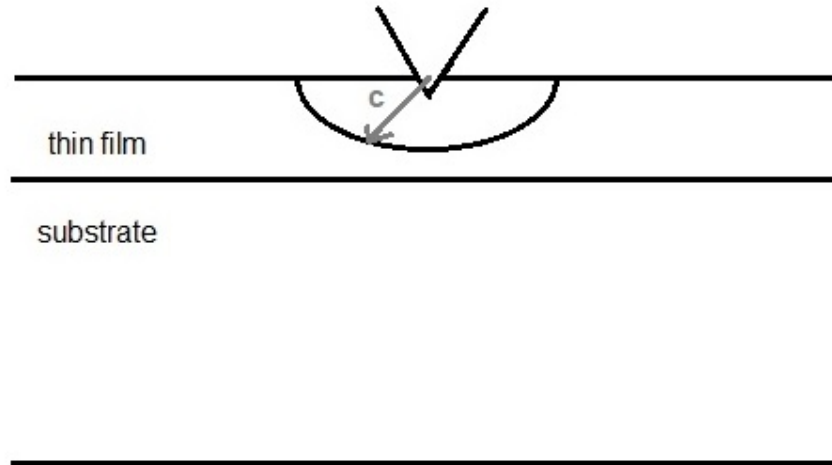


Figure 13: Schematic representation of the plastic zone size.

5 Results

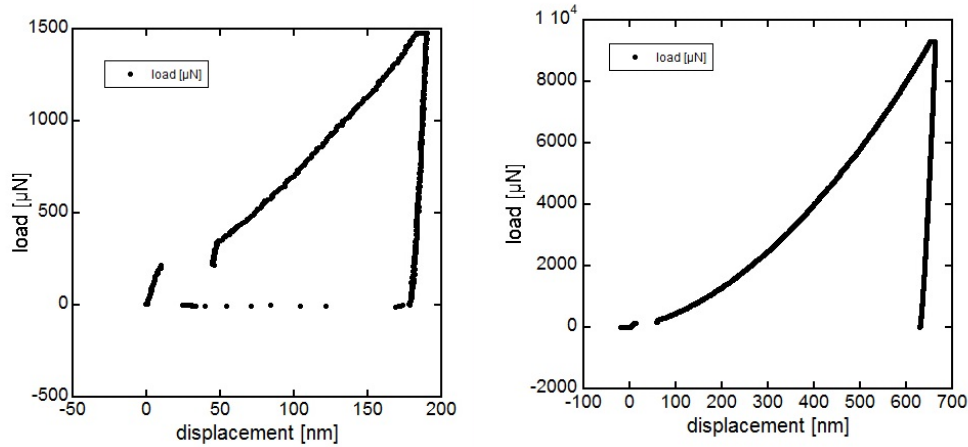
In this section the results from the indentation experiments are presented. First, the bulk samples, Cu and sapphire, are treated and insight about their mechanical response is gained. Later on, the coated specimens with a thickness of 50 nm, 100 nm and 300 nm, are treated with respect to their P- δ curves, hardness and modulus results. These findings are divided into tip and film thickness effects and are examined separately. It will be shown that bulk Cu and the 300 nm thin film provided a large amount of pop-ins. This data will be used to examine the influence of film thickness and tip size on the generation of pop-ins. The amount of dislocations involved in the pop-in events as well as the shear stress, τ_{exc} , required to produce those yield instabilities are calculated.

5.1 Bulk Cu and sapphire indents

Both samples were tested with the standard testing procedure that is used in this thesis. The starting load is 10 mN, which is reduced by 0.5 mN for each indent. Once the test force of 1 mN was reached the load was reduced by 0.1 mN with the load range terminating at a force of 100 μ N. The indentation experiments were carried out using the sharp tip, which has a radius of 300 nm. 100 indents were performed for the bulk Cu sample, whereas 25 tests were run on the bulk sapphire specimen due to the fact that sapphire is very hard and would wear the tip.

5.1.1 Bulk Cu indents

P- δ curves of the bulk Cu is shown in Fig. 14 for maximum loads of 400 μ N and 10 000 μ N.



(a) Load-displacement curve of bulk Cu for a maximum load of 1 mN. (b) Load-displacement curve of bulk Cu for a maximum load of 10 mN.

Figure 14: Pop-ins are frequently found at a displacement below 11 nm with a maximum length of 40 nm.

They resemble the $P-\delta$ curves of a purely plastic indent with a nearly vertical unloading part and residual depths of about 80 and 600 nm and a frequent occurrence of plastic events inside the sample, indicated by pop-ins. They appeared almost exclusively at a displacement below 11 nm, which can be recognized at the beginning of the loading curve. This shallow penetration depth is related to the Hertzian mechanics for a purely elastic contact between two solids. The pop-in length varies between 9 nm up to nearly 40 nm, whereby lengths around 40 nm are more frequent. The hardness on average is 0.9 GPa with a deviation of only 0.034 GPa compared to the literature value of 1 GPa. Experiments provided an average 103.9 GPa as a value for the elastic modulus of Cu with a variation of 4.8 GPa with an assumed Poisson's ratio of 0.3. It fits well with the literature value of 110 GPa [25] with an error of only 5.5 %.

The evolution of hardness and reduced elastic modulus over the contact depth can be seen in Fig. 15 and Fig. 16. The hardness values gradually decrease for larger penetration depths and the modulus exhibits slightly more scatter than hardness.

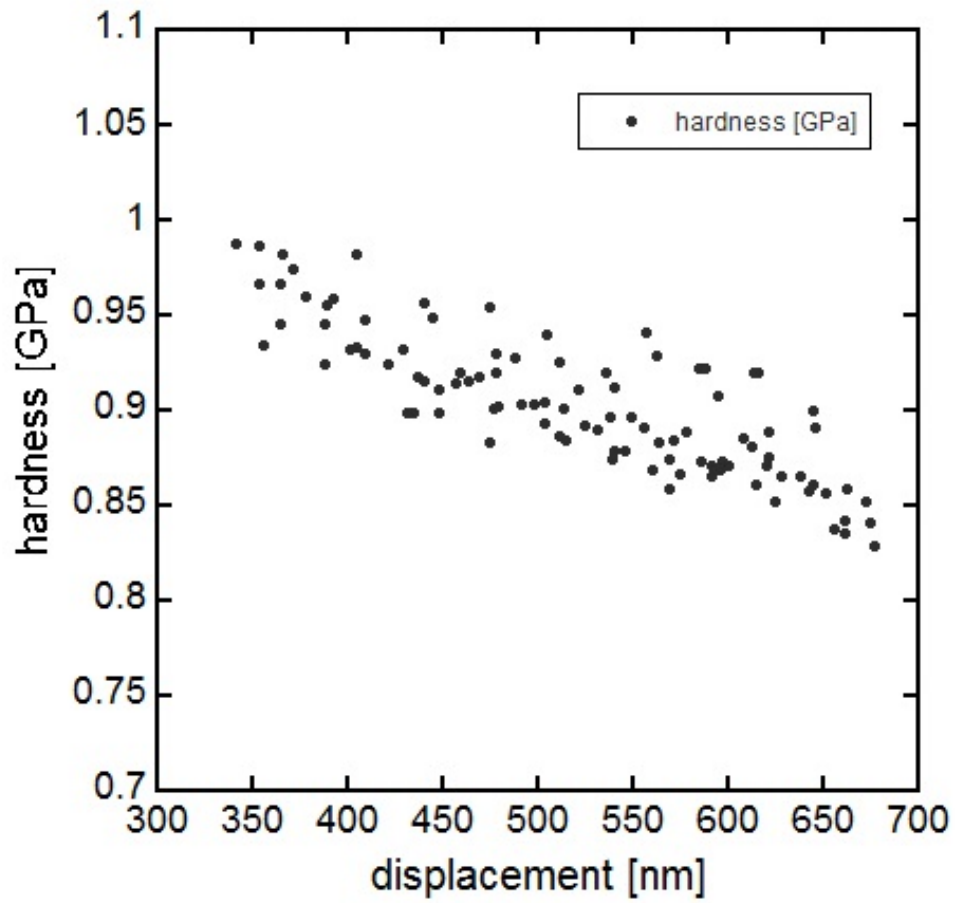


Figure 15: Development of hardness over contact depth. Hardness is slightly decreasing with larger penetration depths but stays well confined between 0.8 and 1 GPa for the displacement range tested.

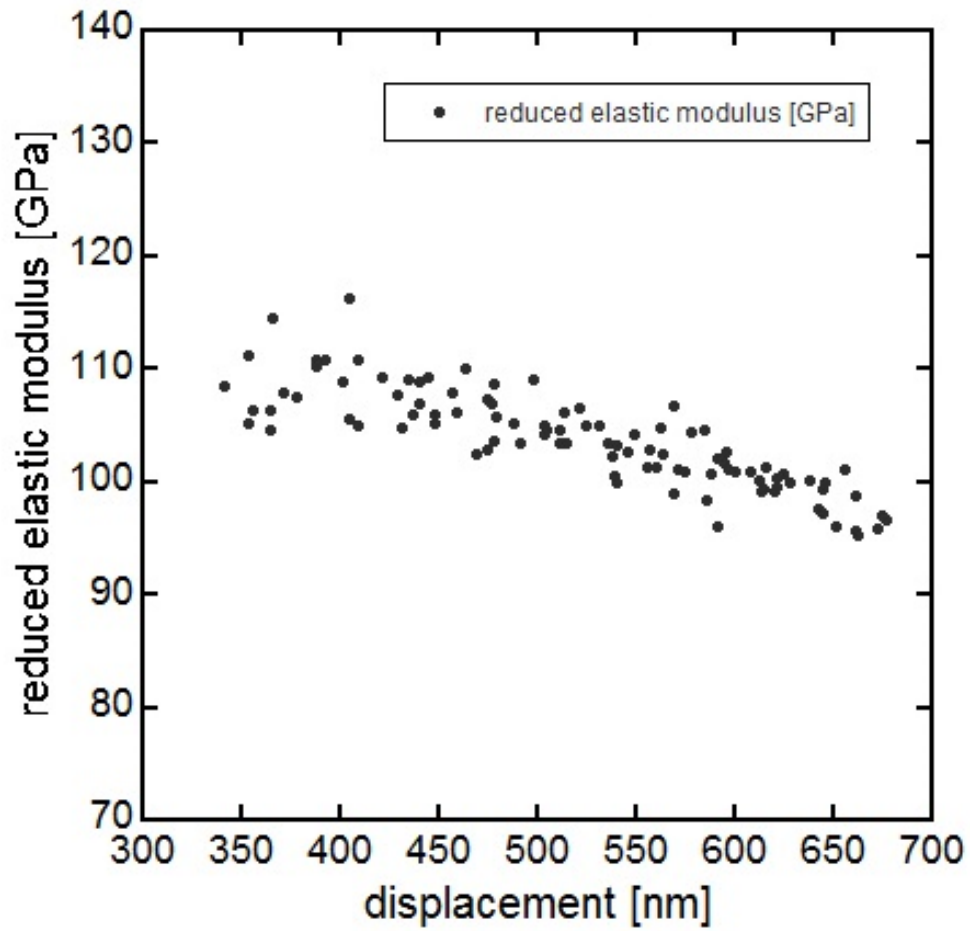


Figure 16: Reduced modulus plotted over contact depth and a range between 120 GPa and 90 GPa. It exhibits slightly more scatter than hardness.

5.1.2 Sapphire indents

In Fig. 17 the P - δ curves of the bulk sapphire specimen are shown.

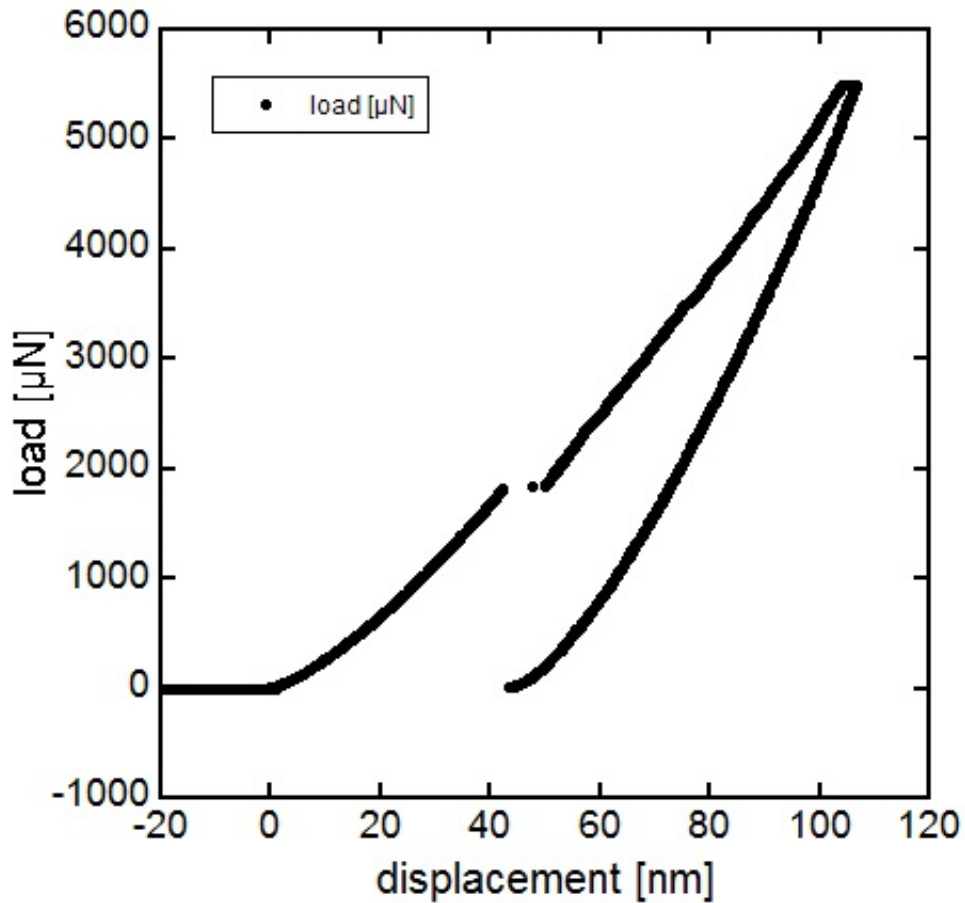


Figure 17: Load-displacement curve for sapphire with fracture events at a displacement of 40 nm.

It shows a steep loading and unloading curve with a permanent displacement of about 40 nm and pop-in events. The occurring pop-ins mark a fracture event inside the sample, which is typical for brittle materials and single crystals. The depth for the permanent imprint is less than for the bulk Cu sample, indicating that for the mechanical response of sapphire the elastic part of deformation is higher. Out of 25 test sets 23 indentations showed pop-ins, occurring almost every time at a displacement of 40 nm with a length range of 7-9 nm. Hardness was measured with 29 GPa with a deviation of 2.9 GPa, which is close to the literature value of 30 GPa [25] incorporating

an error of 7 %. The measured reduced elastic modulus does not reach the literature value of 329 GPa. For a Poisson's ratio of 0.21 calculations provide an elastic modulus of 300 GPa with a deviation of 39.2 GPa.

In Fig. 18 and Fig. 19 the distribution of hardness and reduced elastic modulus over contact depth is displayed. Hardness shows a short plateau at lower penetration depths but decreases constantly after the indicated fracture event. The reduced elastic modulus also follows a downwards trend as its data approaches lower values for larger displacements.

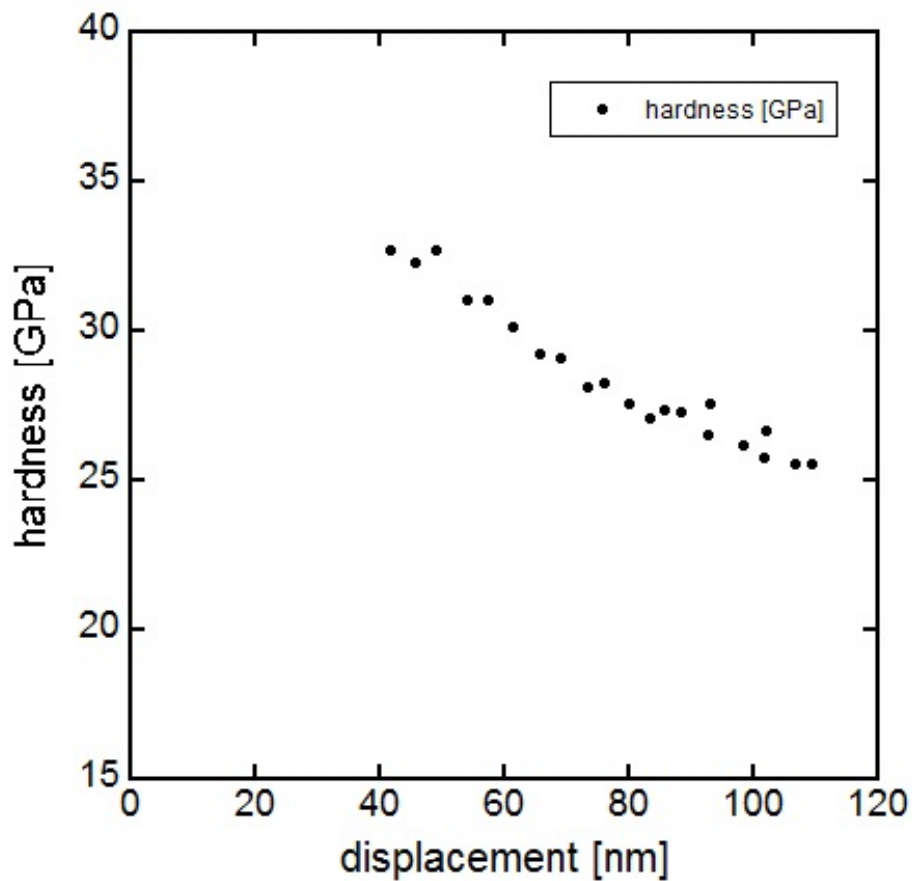


Figure 18: Development of hardness of sapphire over contact depth. It gradually decreases from 34 GPa to 25 GPa with increasing indentation depth.

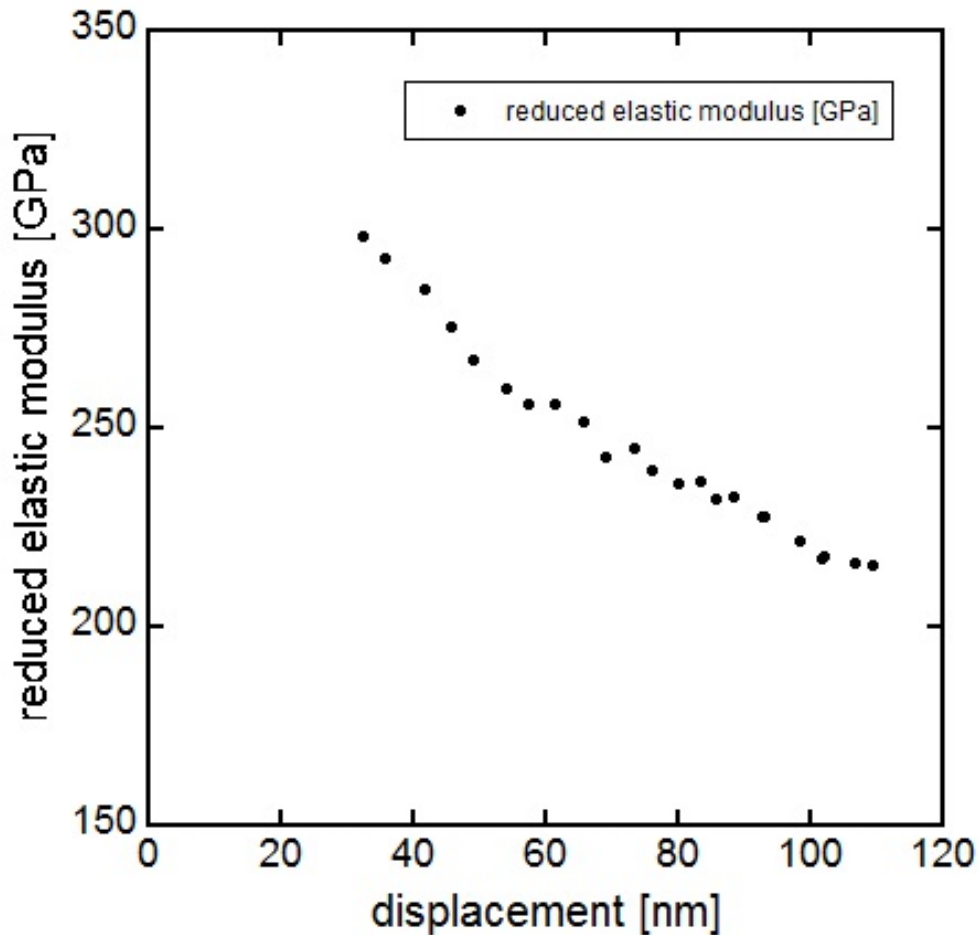


Figure 19: Reduced elastic modulus values for sapphire decrease from 300 GPa down to below 200 GPa with increasing penetration depth.

5.1.3 Summary

The $P-\delta$ curves for the Cu and sapphire bulk sample resemble load-displacement curves for soft and hard materials, given the amount of plastic deformation and elastic recovery [17]. The pop-in events differ in length and occurrence region. The Cu pop-ins happen at smaller displacements and are larger in length, while the sapphire pop-ins are related to fracture events and are shorter and happen farther beneath the surface. The reason for the shorter sapphire pop-ins is that as an ionic crystal sapphire needs to preserve its

charge neutrality. Thus the dislocation movement is restricted since dislocations are a source of a shift in charge in ionic crystals. The values for hardness and elastic modulus are in good agreement with the literature terms for the bulk Cu sample. The resulting hardness for the bulk sapphire specimen matches with literature, but does not agree for elastic modulus. In this paper [26] the value of 440 GPa for the modulus of sapphire is only reached for shallow indentation depths of about 5 nm and decreases with increasing indentation depth. In this thesis we obtain larger displacements and hence lower modulus values.

5.2 Thin film measurements

The coated specimens were tested using the standard procedure in this thesis, introduced in section 4.2. The indentation experiments were carried out on the 300 nm, 100 nm and 50 nm thick thin films on sapphire using the blunt, 1.6 μm radius, and sharp, 300 nm radius, tips resulting in specimen responses that can be related to either tip size effects or influences due to film thickness.

5.2.1 Tip effects

In this section the effects of the different tip radii on the material response are investigated. For each film thickness a representative load-displacement curve with corresponding tip size is displayed. In addition the values of hardness and elastic modulus are investigated, both at the 10 % region and the interface. Moreover, the size of the plastic zone is calculated and compared to the film thickness and plausibility of hardness measurements. The tip area functions were well calibrated using Fused Quartz before indenting the thin film systems.

50 nm film [H]

The P- δ curve for the 50 nm film penetrated by the blunt and sharp tip is depicted in Fig. 20. The curve for the sharp tip depicts a change of the loading slope at a penetration depth of about 50 nm, which is approximately

the interface. For the blunt tip, the change in slope happens at 30 nm, which is slightly before the interface. The slope at smaller displacements is lower and increases with larger penetrations, related to the sapphire substrate underneath. For the sharp tip the difference is even more pronounced with a very flat slope for displacements lower than 50 nm and abruptly rising when the interface is reached. For the blunt tip there were no pop-ins examined, but the sharp tip exhibited some. Their analysis will be treated later. Furthermore, the work of indentation, related to the area circumscribed by the P- δ curve is much smaller for the sharp tip. This is related to the blunt tip not reaching sufficiently high yield stresses as the sharp tip. Thus, the sharp tip causes more plastic deformation as indicated by the larger area beneath the P- δ curve.

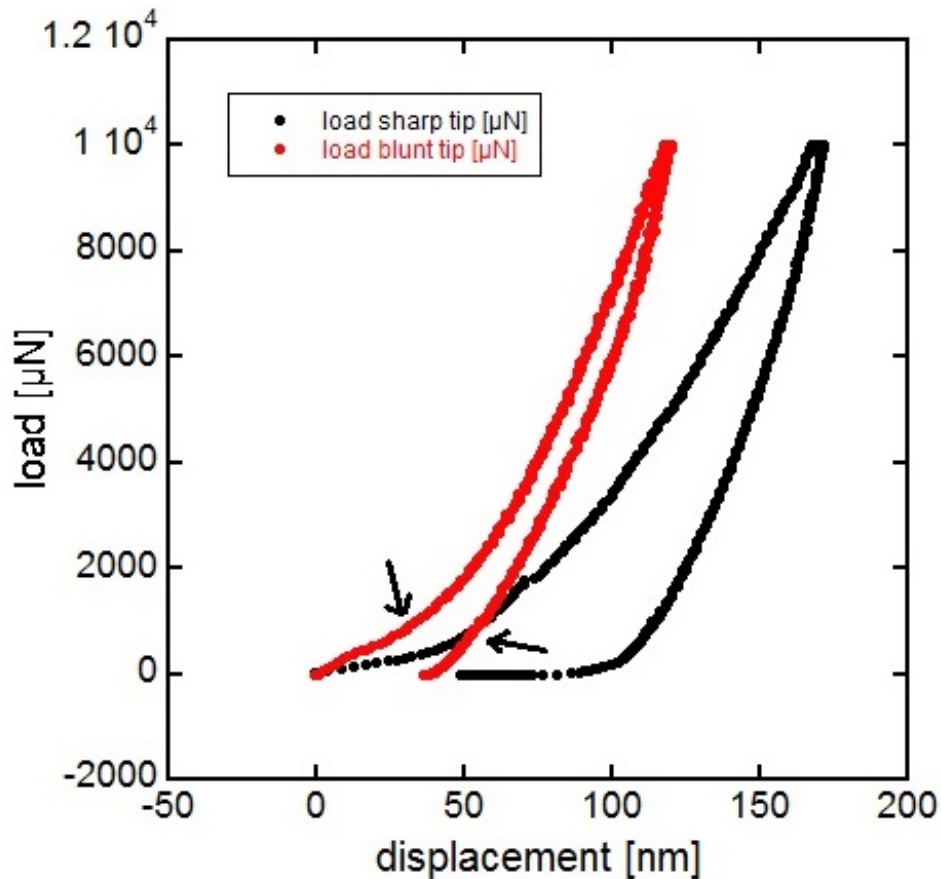


Figure 20: Representative P- δ curves for 50 nm film on sapphire with the blunt and sharp tip. As indicated by arrows a change of the slope of the loading part is visible at displacements of 50 nm for the sharp tip and at 30 nm for the blunt tip. The work of indentation is less for the blunt tip than for the sharp tip.

The hardness values are summarized for the blunt and sharp tip in Fig. 21. The hardness of the sharp tip range from 3.1 GPa for small displacements to 18.1 GPa for large displacement beyond the interface, where predominantly the substrate is measured. For the blunt tip hardness starts at 3.7 GPa and increases to 16.1 GPa for displacements near the substrate region. There is no plateau value reached but rather a continuous increase in hardness. The hardness values at 10 % of the film thickness could only be determined

for the blunt tip with a value of 3.6 GPa. The hardness values are similar until the ratio $\frac{h_c}{t}$ of 1, but start to differ once the indenter displacement reaches the sapphire substrate. It can be seen that the increase is less for the sharp tip with the smaller radius. It is shown in Fig. 22 that the sharp tip generates a smaller plastic zone beneath the indenter than the blunt tip. Hence, the probability of encountering dislocations within the plastic zone of the blunt tip is more likely. This leads to higher stresses during the contact of indenter and specimen and results in a higher measured hardness. The hardness of sapphire, 30 GPa respectively, is not reached but a trend towards it is observed.

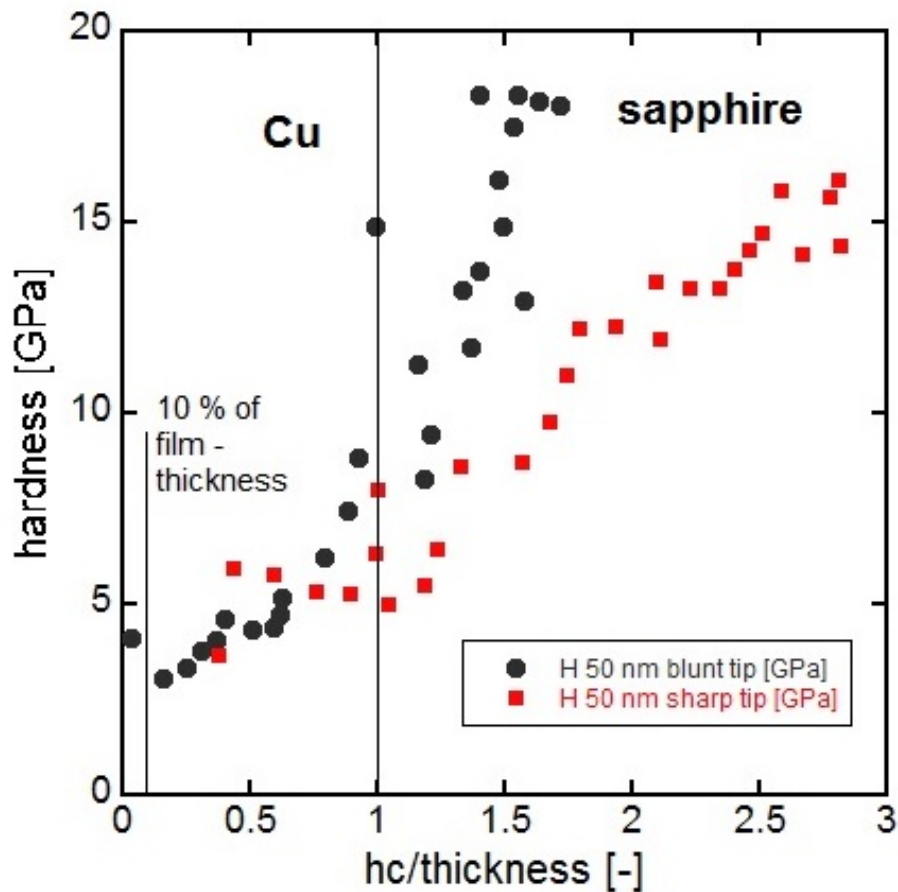


Figure 21: Hardness over $\frac{h_c}{t}$ for the blunt and sharp tip. Hardness starts to differ from that point demonstrating a stronger rise for the blunt tip due to the larger volume tested.

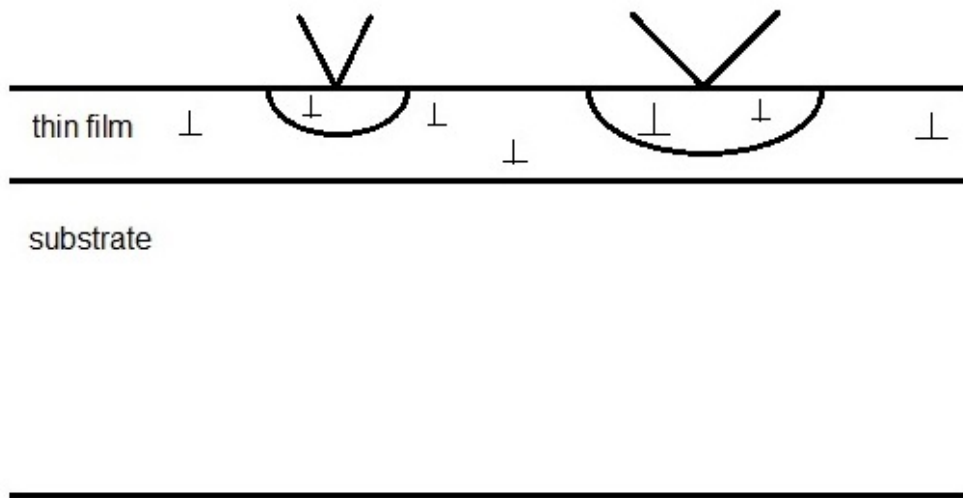


Figure 22: With a sharper indenter the corresponding plastic zone beneath is smaller. The blunt tip has a bigger plastic zone and can activate more stored dislocations, explaining the rise in hardness.

The reduced elastic modulus over $\frac{h_c}{t}$ for the blunt and the sharp tip is depicted in Fig. 23. For the sharp tip an average modulus of 329.8 GPa with a deviation of 48.3 GPa was obtained and for the blunt tip the elastic modulus on average is 311.7 GPa with a deviation of 44.2 GPa. The values exhibit a lot of scatter and it is not possible to obtain a reasonable value for the film only response like it is possible for hardness.

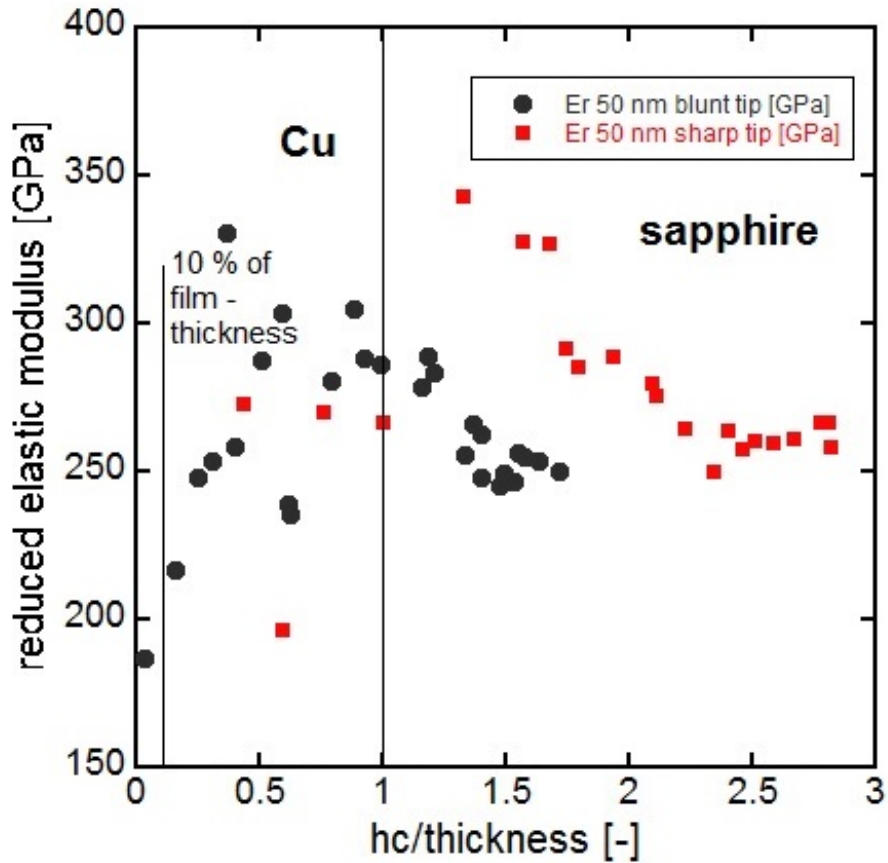


Figure 23: Reduced elastic modulus over $\frac{h_c}{t}$ for the blunt and sharp tip. At $\frac{h_c}{t} = 1$ the interface is reached. The data shows severe scatter.

100 nm film [H]

The P- δ curves of the 100 nm film that have been indented with the blunt and sharp tip is depicted in Fig. 24. Again, the loading curves displays two different slopes parting from a penetration depth around 50 nm for the blunt and sharp tip. Like for the 50 nm film the work of indentation is much smaller for the blunt tip than for the sharp tip. This is also related to the different permanent displacement, which are 40 nm for the blunt tip and 100 nm for the sharp tip, proving that more plastic deformation is reached using the sharp tip. In terms of pop-ins, there are some occurring for the measurements with the sharp tip for regions within the elastic loading

regime and displacements past the interface. They will be treated in detail later on.

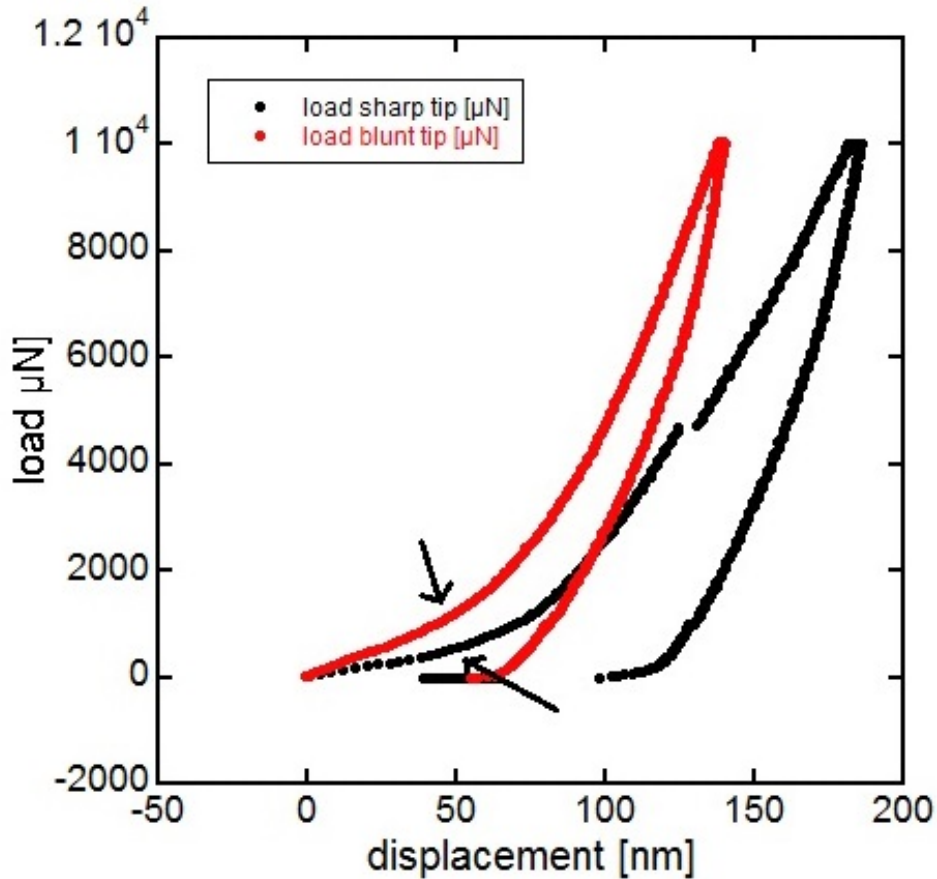


Figure 24: P- δ curves obtained with blunt and sharp tips for the 100 nm film with a change of slope at a displacement of 50 nm, as indicated by arrows. Fracture event happens past the interface. The work of indentation is smaller for the blunt tip than it is for the sharp tip. The remaining displacement is 40 nm for the blunt tip and 100 nm for the sharp tip.

Hardness values over $\frac{h_c}{t}$ for the different tips are shown in Fig. 25. The experimental results for the blunt tip provide values from 2.3 GPa to 13 GPa. For the sharp they range from 3.3 GPa up to 13.3 GPa. At 10 % of the film thickness, 3.7 GPa was determined for the blunt tip, for the sharp tip reasonable measurements started at displacements past the 10

% region. Moreover, there is a plateau region well until 70 % of the film thickness which provides a constant hardness value of 4 GPa for both tips with a deviation of 0.6 GPa. Hardness values start to slightly differ after the 70 % mark and deviate even more once the interface is reached. Like for the 50 nm film, the hardness obtained by the sharp tip rises less past the interface due to the smaller volume beneath the indenter. Again, the substrate hardness of sapphire of 30 GPa is not reached but a trend towards this value is observed.

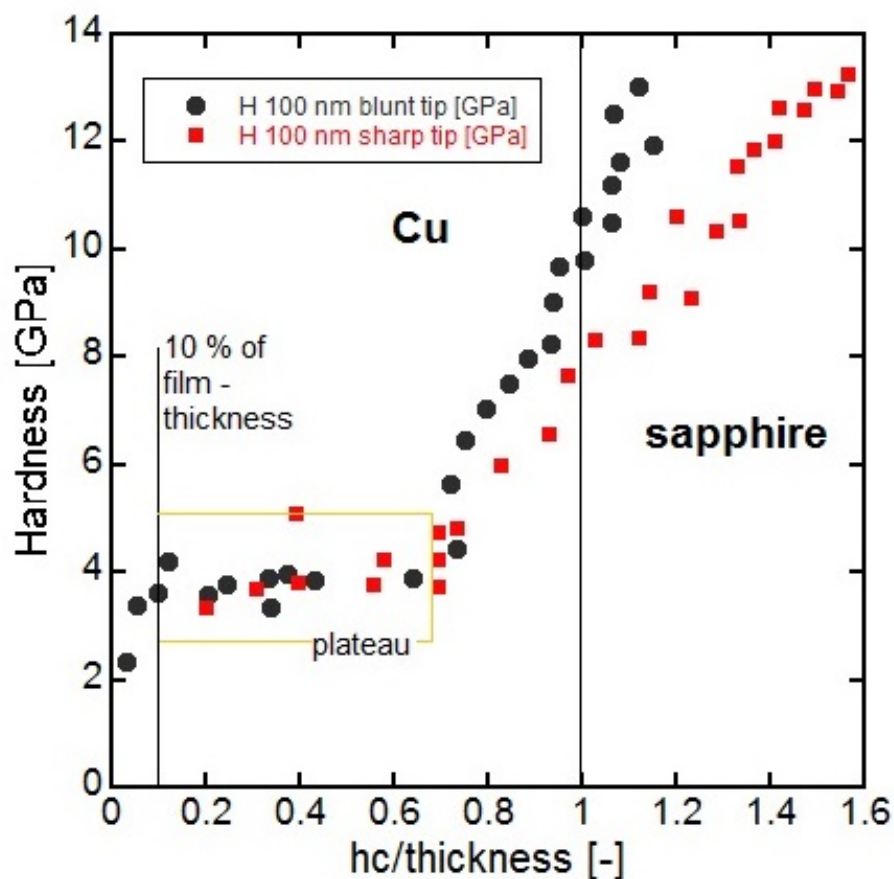


Figure 25: Hardness over $\frac{hc}{t}$ for 100 nm film and the blunt and sharp tip. At a ratio of 1 the interface is reached. Hardness starts to differ from that point, showing a later rise for the sharp tip with trend towards the hardness of sapphire. There is a plateau region for the blunt and sharp tip until 70 % of the film thickness.

The reduced elastic moduli obtained for the blunt and sharp tip are depicted in Fig. 26. For the blunt tip it is determined with 321 GPa with a difference of 55.6 GPa, whereas the sharp tip provides an elastic modulus of 333.1 GPa varying about 54.7 GPa. Again, the scatter is broad, thus rendering it impossible to make a distinct assumption. Of more importance is the fact that at no point bulk Cu values are measured with either tip radius.

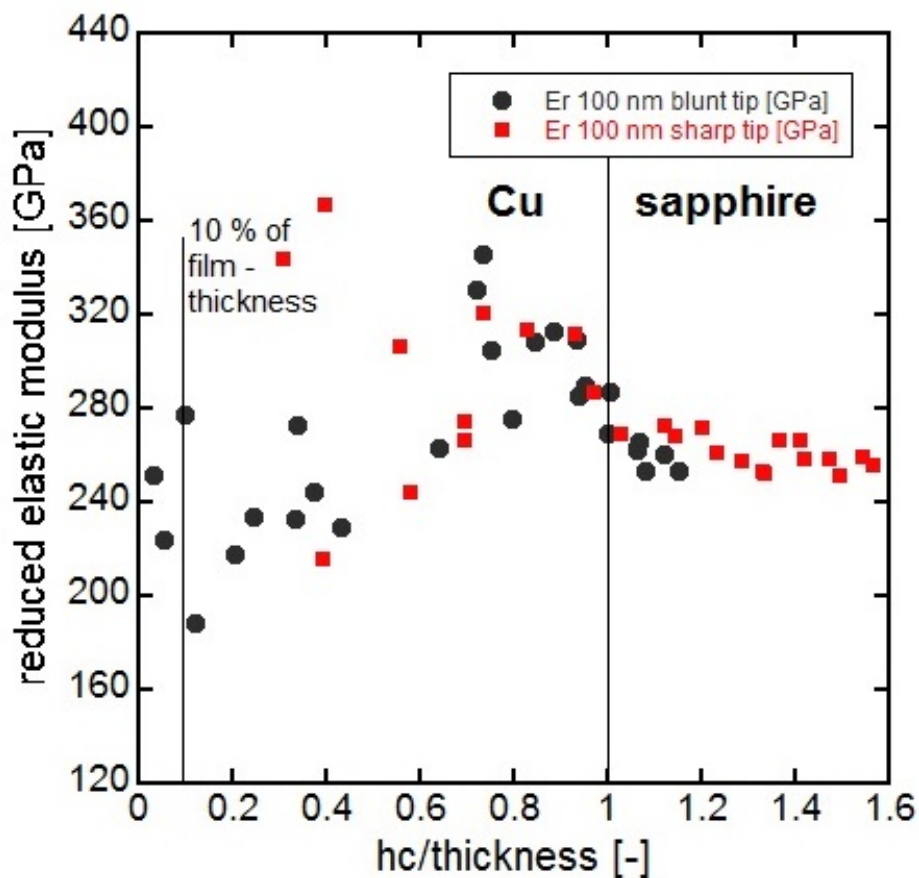


Figure 26: Reduced elastic modulus over $\frac{h_c}{t}$ for 100 nm film and the blunt and sharp tip. At $\frac{h_c}{t} = 1$ the interface is reached.

300 nm film [H]

The P- δ curves for the 300 nm film indented with the blunt and sharp tip are shown in Fig. 27. No change in the loading slopes is observed due to

the tips not penetrating the interface region with the applied test force, thus resembling the P- δ curve of bulk Cu. Several pop-ins occur for the blunt and the sharp tip, which will be discussed in detail later. The work of indentation is similar for both tips, resulting in only a slight difference for the permanent displacement, 240 for the blunt tip and 270 for the sharp tip respectively.

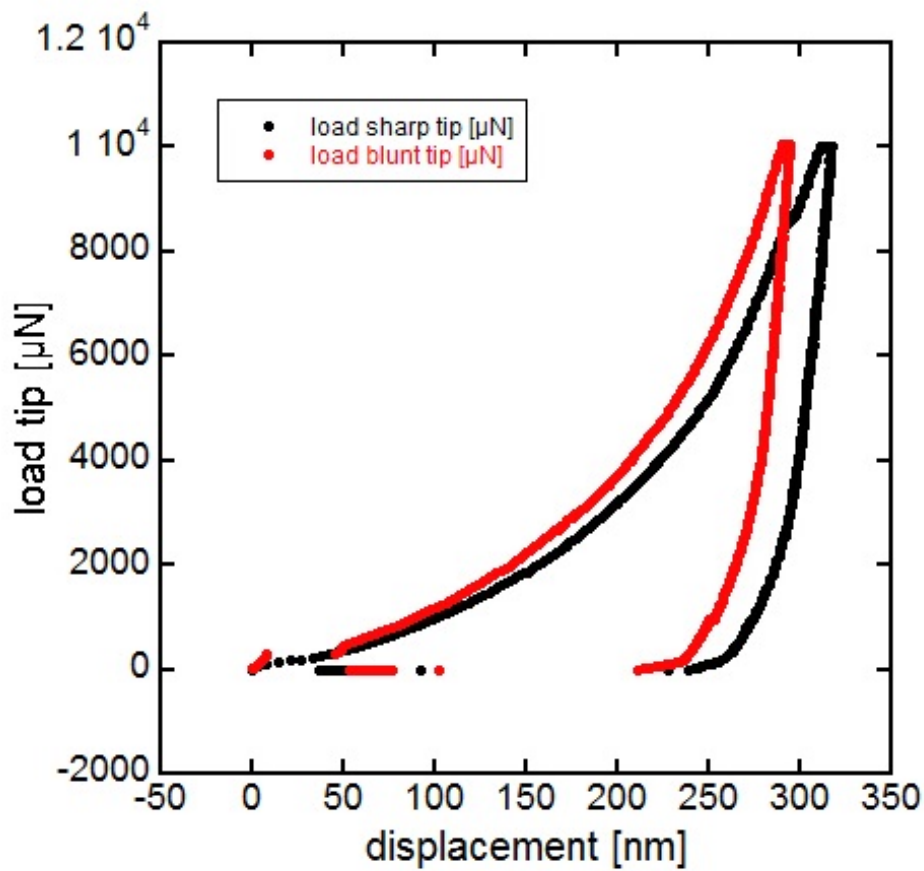


Figure 27: P- δ curves for the blunt and sharp tip. No change in slope is observed and the works of indentations are similar. With the present displacements the interface is just reached but not the substrate. Pop-ins are occurring.

The hardness values, shown in Fig. 28 are also similar, only with the data of the blunt tip being lower than the data for the sharp tip for displacements smaller than 70 %. For the blunt tip hardness on average was 2.1 GPa and

for the sharp tip it was 2.9, which is 233 - 322 % higher than for the bulk Cu sample, which displayed a hardness of 0.9 GPa. The interface is only just reached, but influences the hardness values to face an upward trend at about 70 % of the film thickness. Below that, however, hardness is similar for both tip sizes and only changes slightly until 70 % of the film thickness. At 10 % of the film thickness hardness values are 2 GPa for the sharp tip and 1.6 GPa for the blunt tip with a deviation of 0.2 GPa for the blunt tip.

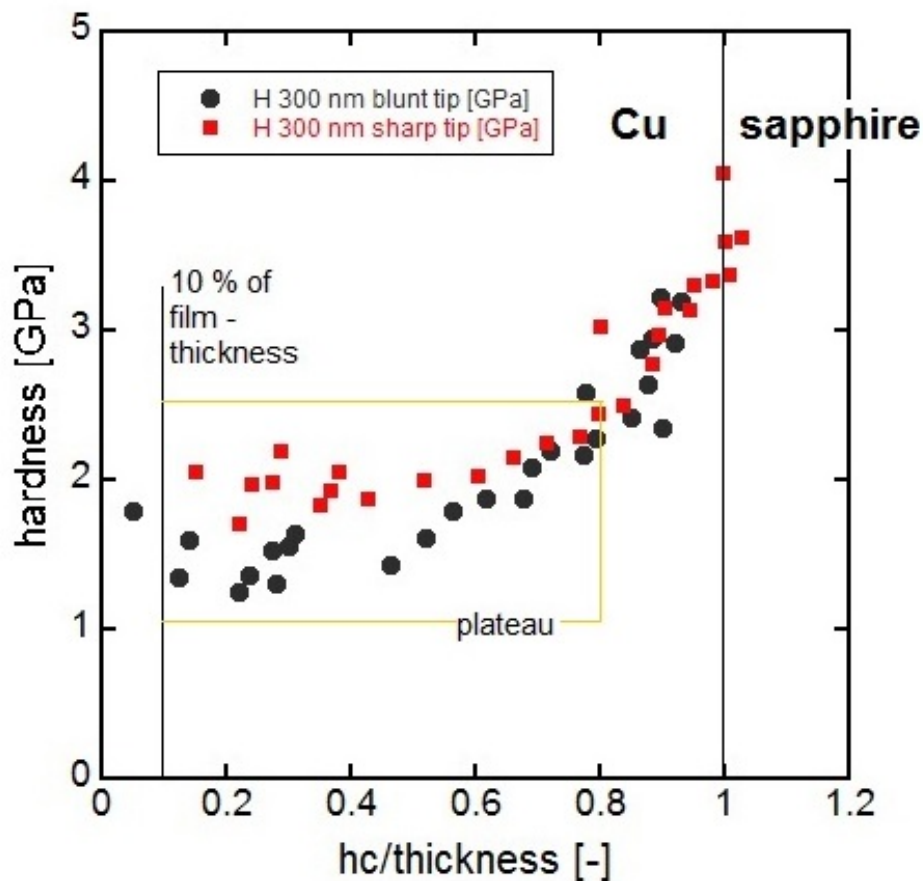


Figure 28: Development of hardness over $\frac{hc}{t}$ for both tip sizes. A constant value of hardness is obtained until 70 % of the film thickness before an upward trend is induced by the substrate.

The reduced elastic moduli are depicted in Fig. 29. The elastic moduli are obtained with 239.7 GPa with a deviation of 63 GPa for the blunt tip and with 287 GPa for the sharp tip varying about 76.8 GPa.

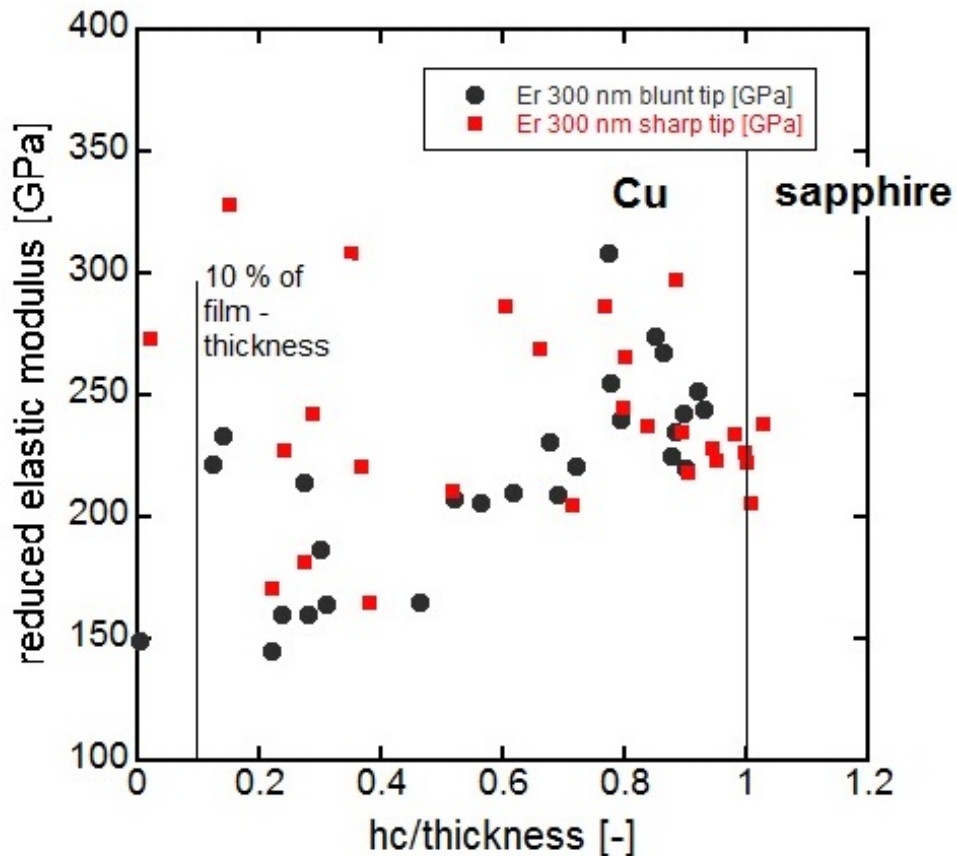


Figure 29: Development of elastic modulus over $\frac{h_c}{t}$ for both tip sizes. The huge scatter renders it impossible to consistently determine the elastic modulus.

Summary [H]

The different tip sizes caused very diverse mechanical responses within the coated samples. The slope of the loading curve depicted a change for both tips for the 50 nm and 100 nm thin films due to penetrations beyond the interface and therefore the presence of the substrate was felt. The 300 nm film showed no change in the slope for either tip because only the thin film

was tested and the displacement never reached past the interface. Also for the 50 nm and 100 nm thin film the work of indentation severely differed with it being smaller for the blunt tip due to larger elastic volume present under the indenter, resulting in less permanent displacements. This was not observed for the 300 nm thin film with the work of indentation being equal for the sharp and blunt tip. This can again be related to the displacement not reaching past the interface and therefore not having an influence of the substrate.

Tab 1 provides an overview of the hardness values from the different samples at 10 % of the film thickness and at the plateau region if either was observed. The depth of useable hardness data scales with increasing film thickness. The 50 nm film does not display a proper plateau value, the 100 nm film exhibits a constant hardness value up to 70 % of the film thickness and the 300 nm film allows a proper hardness evaluation until 70 % of the film thickness. Moreover, there is a reasonable agreement for hardness values for both tips.

Table 1: Hardness values overview for the sharp tip

sample	sharp tip		blunt tip	
	H [GPa] 10 %	H [GPa] plateau	H [GPa] 10 %	H [GPa] plateau
50 nm	-	-	3.6 +/- 0.7	-
100 nm	-	4 +/- 0.6	3.7 +/- 0.4	4 +/- 0.6
300 nm	2	2 +/- 0.2	1.6 +/- 0.2	1.7 +/- 0.4
bulk Cu	-	0.9	-	0.9 +/- 0.1

In Fig. 30 the comparison of hardness for 10 % of the film thickness and the hardness value of the plateau region for the different film thicknesses and bulk Cu for the sharp tip are provided. The 50 nm film did not display a plateau value, but hardness remained constant up to 60 % and 70 % for the 100 nm and 300 nm thin films. Moreover, no proper hardness values at 10 % could be determined for the thinner films due to the sharp tip quickly reaching the interface, however for the blunt tip it was possible in all cases, yet the determined values differ up to 300 % from the value obtained for

bulk Cu, indicating that even at small penetrations the hardness of thin films does not drop to bulk Cu values. This is will be further treated in the next section.

If the thin film is thick enough, the hardness can remain constant for a plateau region up to 60 - 70 % of the film thickness, making it possible to extract proper hardness values even beyond 10 % of the film thickness. The elastic modulus were never reasonable for bulk Cu and much nearer to the sapphire substrate.

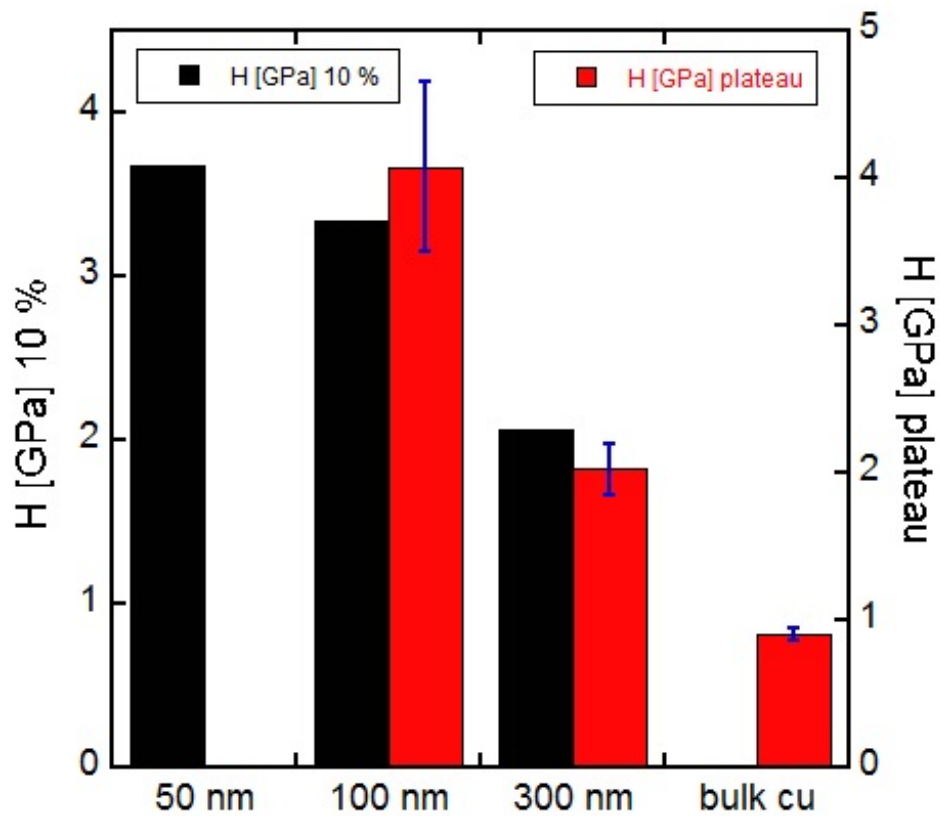


Figure 30: Hardness values comparison for 10 % of the film thickness and plateau region plus standard deviation for the sharp tip.

In Tab. 2 an overview of the elastic moduli for tip size and sample is depicted. In general the scatter is high and does not display a proper

agreement between the values or reasonable values for the Cu film. With increasing film thickness the deviation rises too, whereas the elastic moduli values decline. These results provide evidence that the 10 % rule of thumb should not be applied to extract the elastic modulus values for thin films.

Table 2: Elastic modulus overview

sample	E [GPa] blunt tip	+/-	E [GPa] sharp tip	+/-
50 nm	311.7	44.2	329.8	48.3
100 nm	321	55.6	333.1	54.7
300 nm	239.7	63	287	76.8
bulk Cu	103.8	4.3	103.9	4.8
bulk sapphire	300	39.2	255.3	41.1

Fig. 31 provides a graphic overview with deviation for the estimation of each elastic modulus, further indicating that a reasonable agreement cannot be obtained, since the elastic moduli values are much closer to sapphire.

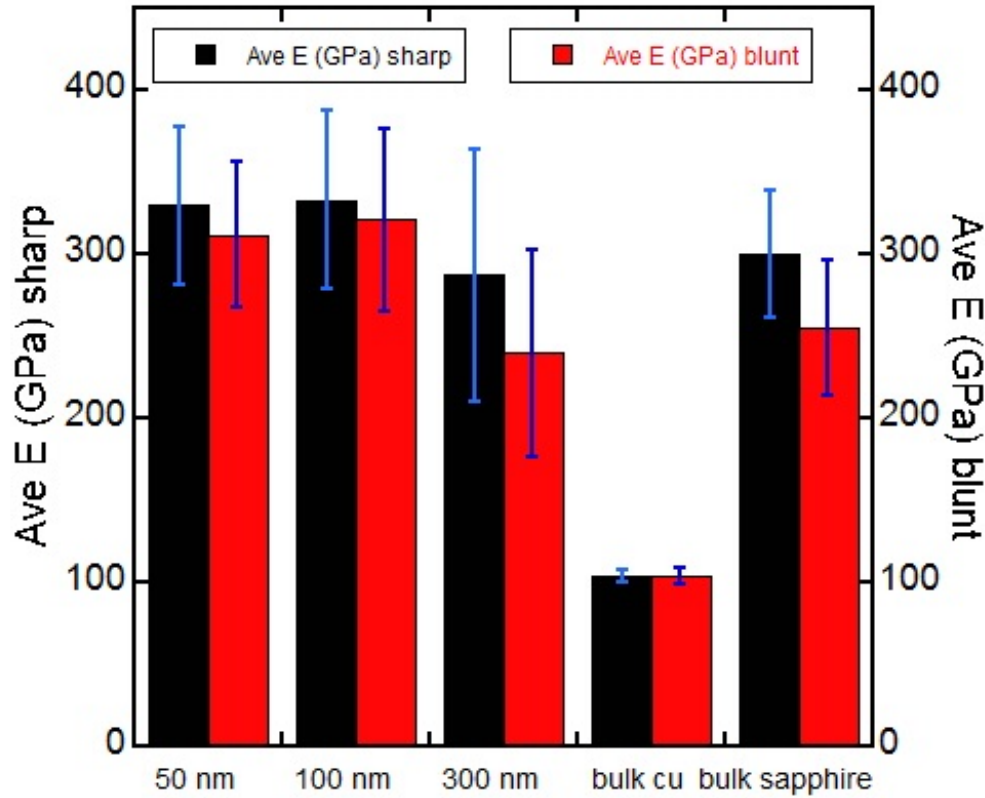


Figure 31: Elastic modulus comparison for the blunt and the sharp tip.

5.2.2 Film Thickness Effects

In Fig. 32 representative $P-\delta$ curves with a maximum load of $1100 \mu\text{N}$ for the 50 nm, 100 nm and 300 nm films are depicted. They were tested with the TriboIndenter PI 950 using only the sharp tip. The $P-\delta$ curve of the 50 nm thin film exhibits the earliest slope change with the steepest rise out of all three curves, which is related to the substrate being closest out of all coating-substrate systems. The work of indentation is also smallest for this thin film and the permanent displacement is about 45 nm. The slope of the 100 nm thin film also rises very steeply, however, not as much as the slope of the 50 nm film due to the film being thicker (100 nm vs 50 nm). The work of indentation is also slightly larger and the permanent displacement

is about 60 nm. The P- δ curve of the 300 nm thin film is similar to an almost purely plastic imprint, resembling bulk Cu load-displacement curves. The occurrence of pop-ins and the nearly vertical unloading slope emphasise the plastic behaviour.

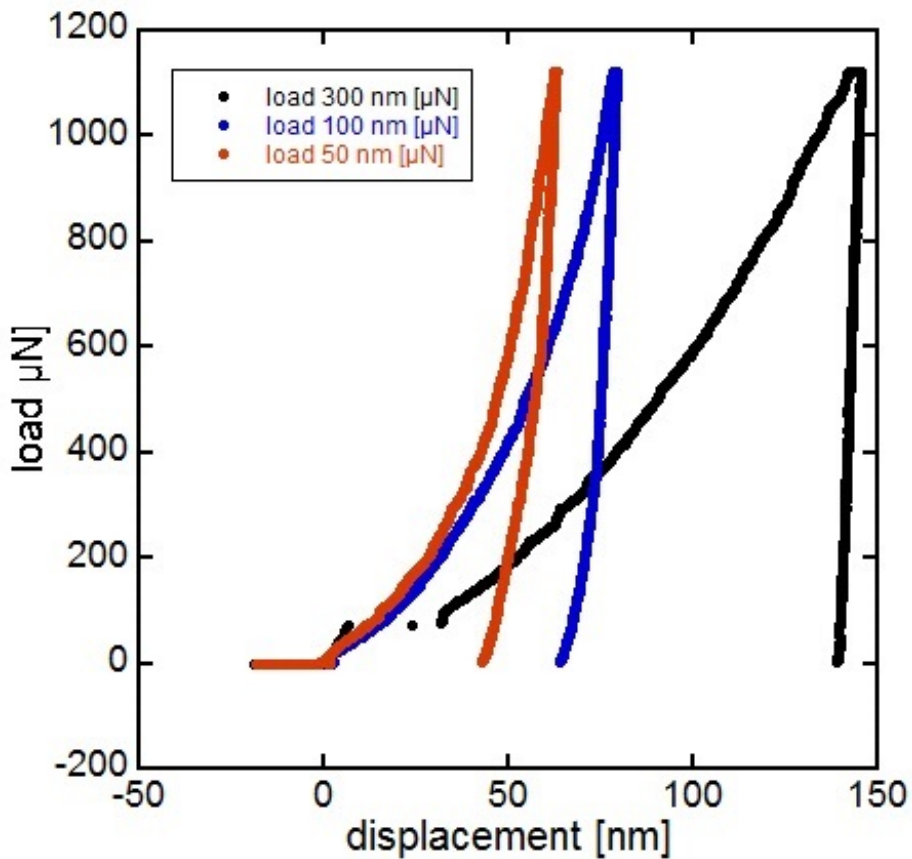


Figure 32: P- δ curves for different thicknesses indented with the sharp tip. The 300 nm film shows pop-in events at a displacement below 10 % of film thickness.

All combined hardness values over $\frac{h_c}{t}$ are shown in Fig. 33. It is observed that the hardness of the 300 nm film remains fairly constant until about 70 % of the film thickness with about 2.2 GPa \pm 0.3 GPa, which is in good agreement with the behaviour measured in section 5. Also, the displacement obtained with this film only reaches the interface but not past it. At 70 %

some first influences related to the substrate are felt and show a further upwards trend for larger displacements. The 50 nm and 100 nm film do not show a plateau for this data and the obtained penetration depths reach well beyond the interface. More indents at shallower depths are necessary for a full examination. The strong substrate effect leads to hardness continuously rising, from 5.8 GPa towards 17.3 GPa for the 50 nm film and 4.3 GPa up to 14.1 GPa for the 100 nm film. The hardness values for the 100 nm film are not only lower but the indenter also does not reach the same large displacements. This indicates a stronger influence from the substrate for the 50 nm and is confirmed by a higher hardness at maximum displacement. Although the actual hardness of the substrate, that is to say 30 GPa, is not reached in any of the samples, a trend towards it is observed. It likely requires deeper penetrations to measure the correct hardness so the thin film is negligible. Considering the opposite case, hardness at 10 % of the film thickness respectively, it should be emphasised that neither was the proper bulk hardness of Cu determined for any film-substrate system, nor was the hardness similar between the different samples. The different film thicknesses can be considered as grains with the corresponding grain sizes of 50 nm, 100 nm and 300 nm. The Hall-Petch law [27] [28], which is also valid for thin films on substrates, expects higher hardness for smaller grains. Therefore, the hardness values should not be similar between the different samples nor should they provide bulk Cu values. According to the hardness measurements of the different films it is observed that the useable hardness data scales with increasing thickness, meaning that the thicker the film the more likely it is to determine realistic values.

Furthermore, it is found that the thicker the film, the less the rise in hardness. This can be related to the Hall-Petch law, which states a higher hardness for smaller grains. Due to the dislocation movement being confined inside the grains and the reinforced repulsion between them an increase in hardness is caused. Nix [29] explained this phenomena for single crystals thin films stating that dislocations are confined to move within the film and cannot migrate into the substrate, which causes a misfit dislocation to be deposited

at the interface. Soare and Bull [30] stated that for thinner films a significant rise in hardness is observed, which is in agreement with the study of this thesis.

Although the 100 nm thin film did not display a plateau with this set of data like it did in section 5, the 300 nm repeated its behaviour with hardness being constant up to 70 % of the film thickness. This suggests that the 10 % rule of thumb is still valid for hardness as initially described by Bückle in section 2 and it can be extended for larger ratios, however, only if the film has a suitable thickness. Furthermore, this would only account for soft films on hard substrates. Hard films on soft substrates would perform differently and should be examined separately. For thinner films it is not suggested to apply the 10 % rule of thumb for hardness, since the film thickness or grain size in terms of the Hall-Patch law is the limiting factor. As already depicted in section 5.2.1 the plastic zone size builds underneath the indenter. For thinner films (50 and 100 nm) the size of the plastic zone is not confined to the films but reaches into the substrate. Only for films of 300 nm and larger can the plastic zone fully build and allow for reasonable hardness measurements.

For the sake of completeness the determined elastic moduli for each film are listed in Tab. 3 and show more scatter with increasing film thickness. Overall the findings were the same as in section 5, that nanoindentation does not provide suitable data, not even within 10 % of the film thickness. This will be treated in detail in a later section.

Table 3: Elastic modulus overview

sample	E [GPa]	+/-
50 nm	359.5	14.9
100 nm	364.5	34.9
300 nm	275.8	45.7

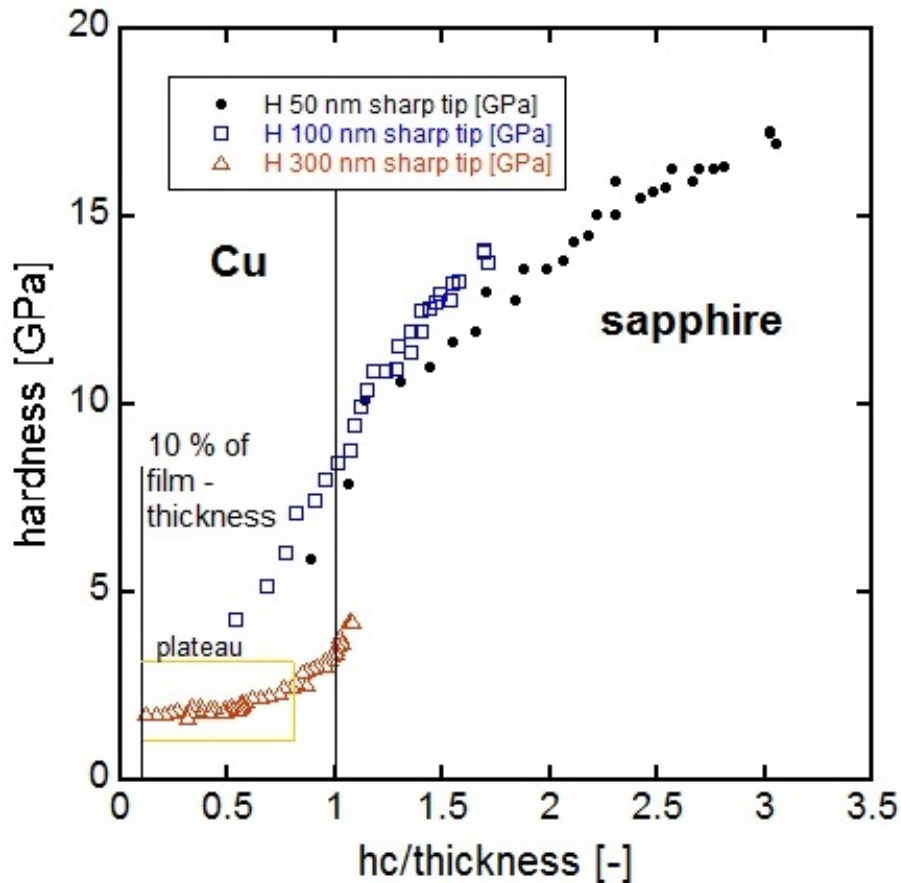


Figure 33: Hardness over contact depth for the 50 nm, 100 nm and 300 nm thin films. The 300 nm film exhibits a plateau until 80 % of the film thickness, whereas the 100 nm and 50 nm thin film are influenced by the substrate.

5.2.3 Summary

The behaviour of the thin films depends on the tip size and the thickness of the film, which can be regarded from the different $P-\delta$ curves. Whereas the substrate effect is strongly observed in the corresponding curves for the 50 nm and 100 nm sample, the $P-\delta$ curve of the 300 nm sample resembles that of bulk Cu. Another main difference would be the occurrence of pop-ins, which was more abundant for a thick film and shall be treated in detail in

the following section.

Hardness again provided interesting results with respect to the film thickness. There is a strong influence from the substrate felt for the 50 nm and 100 nm sample, with hardness not dropping to bulk values for even the lowest loads. In comparison to the former section, where hardness displayed a constant value up to 60 % of the film thickness, this time no plateau was obtainable for either film thickness, reinforcing the need for thicker films to obtain proper data. For the 300 nm film, however, hardness again remained useable until well 70 % of the thickness. It did not drop to bulk values even for lowest loads, displaying a deviation on average of 232 %.

In terms of film thickness, it is evident from the obtained data, that hardness scales inversely with thickness. This is similar to the Hall-Patch law, which states higher hardness for smaller grains. In our case, the single crystal films can be seen as grains with a grain size to corresponding film thickness. Thus, the 50 nm coating comprises a higher hardness than the 300 nm sample.

5.3 Pop-in analysis

As explained in earlier sections the appearance of pop-ins is related to the plastic behaviour of the investigated specimen as dislocations are activated and material flows away from the indenter. The frequency, length and range of initiation of pop-ins strongly depend on the sample system, whereas tip size influences are secondary. As a consequence assumptions about the plastic behaviour of the different specimens can be obtained.

In Tab. 4 and 5 the range of initiation, length and frequency of all samples indented with the sharp and blunt tip are listed. For the 50 nm film no pop-ins occurred. The 100 nm film exhibited several pop-ins only when indented with the sharp tip. It should shortly be mentioned that for the 100 nm film pop-ins were formed twice: once at shallow indentation depths below 10 nm and the other time at a displacement of about 125 nm. The latter can be

related to fracture events inside the substrate and do not characterize the thin film behaviour, which is why only the pop-ins at shallow displacements were examined. The 300 nm thin film exhibited pop-ins for both tips, as did the bulk Cu sample. For the sapphire substrate pop-ins were only observed for the sharp tip.

According to the appearance of pop-ins it can be stated that their occurrence is almost equally likely when the specimen is indented with a sharp or a blunt tip. The changes in frequency are only minor for the different samples and tips, however, it can be stated that the blunt tip generates more pop-in events than the sharp tip. This can be observed from Tab. 4 and 5 especially for the 300 nm sample and bulk Cu. An explanation for the higher frequency obtained with the blunt tip would be that the larger indenter area encounters more stored dislocations within the sample and thus generates more pop-in events.

Furthermore, it can be said that the bulk Cu exhibits the longest pop-in events. Although the 300 nm sample comes close in length, there is still a higher fraction of longer pop-ins found for the bulk Cu sample. This observance is independent of the tip radius. A possible explanation for this can be the constraint imposed by the substrate. Pop-ins are characterised by material flowing away from the indenter once dislocation avalanches are activated. If there is a stronger substrate underneath the material flow is prohibited, thus stopping the dislocation movement and shorten the length of pop-ins.

A discrepancy arised from the pop-in analysis of sapphire since it exhibited pop-ins for the sharp tip but not for the blunt tip. The reason for this behaviour might be that, as a brittle material, sapphire is likely to fracture when submitted to external stresses. This requires a certain amount of stress in order to happen. Since the sharp tip with a smaller area underneath the indenter is capable of generating higher stresses than the blunt tip it could cause fracture events inside the sapphire specimen more easily.

Table 4: Pop-in overview for the sharp tip

sample	initiation [nm]	length [nm]	frequency out of 28 [-]
50 nm	-	-	-
100 nm	1-3	7-10	2
300 nm	5-10	10-39	22
bulk Cu	4-12	6-47	85 (out of 100)
bulk sapphire	39-45	5-9	23 (out of 25)

Table 5: Pop-in overview for the blunt tip

sample	initiation [nm]	length [nm]	frequency out of 28 [-]
50 nm	-	-	-
100 nm	-	-	-
300 nm	10	4-36	26
bulk Cu	5-16	4-47	24
bulk sapphire	-	-	-

Based on the pop-in data obtained from Tab. 4 and 5 the shear stress, τ necessary to activate the dislocations and, incorporating the Burgers vector, b , the number of dislocations responsible for the material flow can be examined. The values for τ_{exc} are in the range of Gigapascals, which matches with statements found in literature [20]. An overview about the average shear stresses necessary to generation pop-ins, τ_{exc} , is provided in Fig 34.

Table 6: Shear stresses and number of dislocations for the sharp tip.

sample	τ_{exc} [GPa]	number of dislocations [-]
50 nm	-	-
100 nm	7-9	56-85
300 nm	2.9-8.89	84-354
bulk Cu	3.071-5.75	85-364
bulk sapphire	21.31-23.57	13-20

The results are given in Tab. 6 and are calculated from Eqn. (12) and from the pop-in length divided by the Burgers vector, b . The Burgers vector was obtained considering the lattice constant, a , respectively c , of Cu (fcc) and sapphire (hcp). For Cu this is $a=0.255$ nm and for sapphire $c=1.299$ nm in z-axis direction [31] [32]. Incorporating the relation of $b = \frac{a}{2}$ and $b = \frac{c}{3}$. This provided a Burgers vector of 0.1275 nm for fcc Cu and 0.433 nm for hexagonal sapphire in the z-axis direction.

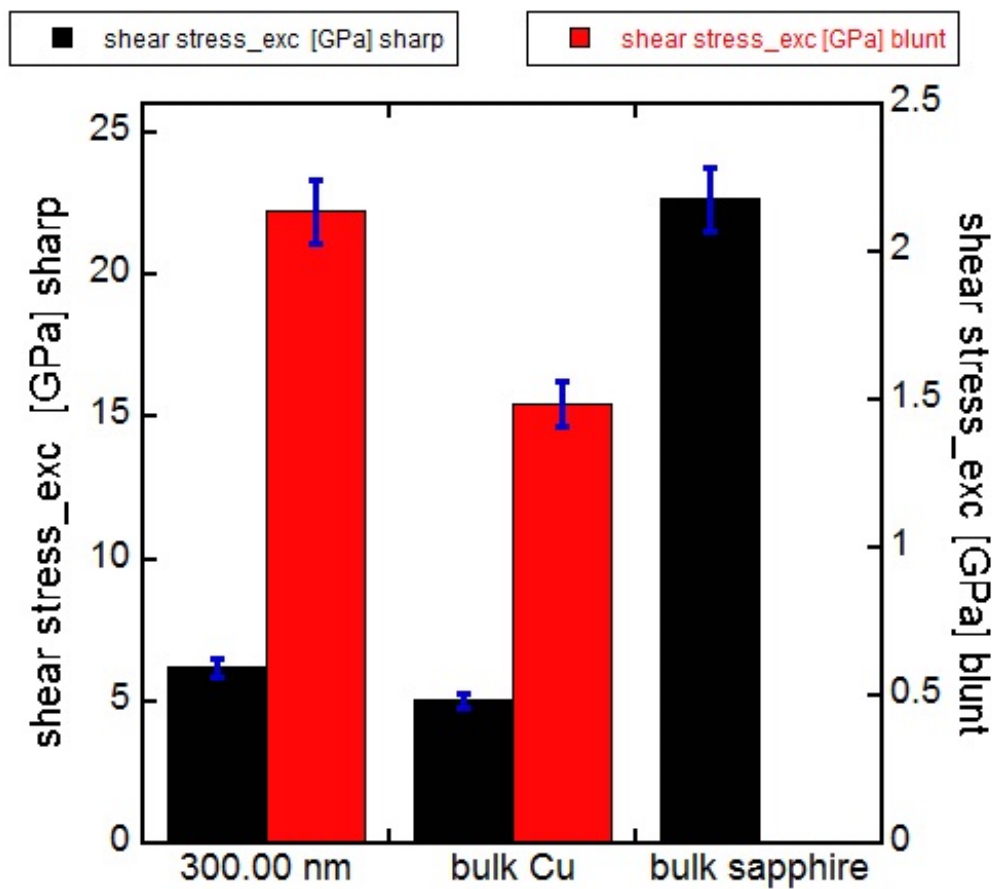


Figure 34: Overview of shear stresses necessary to generate pop-ins with the y-axes displaying the shear stresses for the blunt and sharp tip.

6 Discussion

6.1 Effect of Pile-up

It was already mentioned in section 3.1.1 that the Oliver-Pharr method is well suited for the testing of bulk materials, as long as pile-up does not occur with the tested samples. Generally the Oliver-Pharr method works poorly for the characterisation of thin films, amongst others because it does not account for pile-up. As found in other studies [21] the problem was remedied by measuring the actual contact area from SPM images. This procedure was applied in this thesis by imaging indents and measuring the actual contact area using ImageJ, as introduced in section 4.2. The result is graphically depicted in Fig. 35 for the 50 nm film indented with the blunt tip.

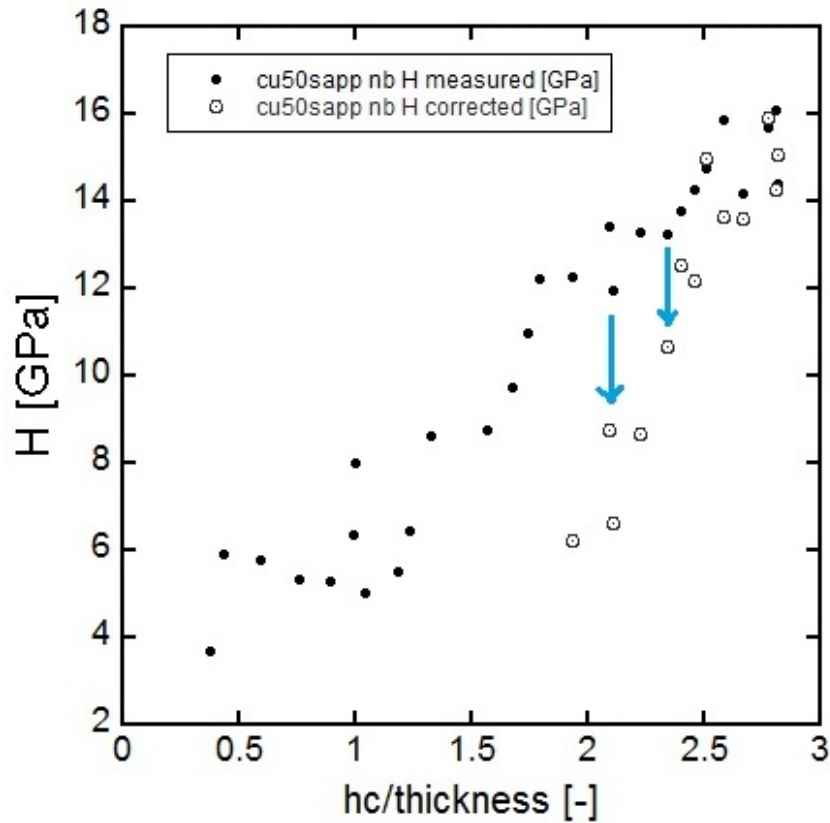


Figure 35: Corrected hardness for the 50 nm film indented by the blunt tip. Hardness dropped to lower values after the correction as indicated by the arrows. For $\frac{h_c}{t} = 2$ and above corrected and uncorrected hardness values are similar.

Corrected hardness values are only obtainable from $\frac{h_c}{t} = 2$ and above since it gets increasingly difficult to obtain pictures of indents with lower loads due to imprints becoming beyond recognition. Nonetheless, hardness is initially lower, proving that it was in fact initially overestimated but joins the uncorrected data for values of $\frac{h_c}{t}$ far past the interface, where mainly the substrate is measured.

In terms of pile-up around the indent it was found that pile-up height increased with increasing penetration depth. A possible explanation could be the consideration of hydrostatic pressure, that is available for material

inside the bulk, but is absent for material at the surface. When the indenter is pressed into contact with the material, a plastic zone is generated according to the tip size and shape. This zone creates stresses and presses against the surrounding material. As a consequence of *actio est reactio* forces acting against those stresses are generated. Since there are no counteracting forces on the surface, the material does not encounter resistance and is pulled upwards. This phenomenon scales with increasing stresses, with increasing indenter load and thus increasing penetration depth respectively.

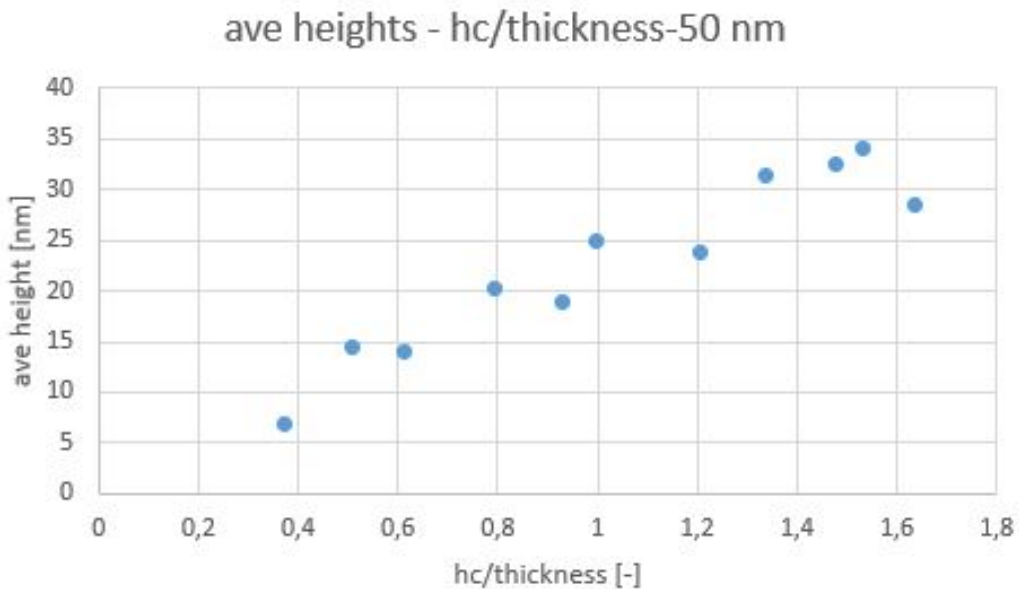


Figure 36: Development of pile-up height over $\frac{h_c}{t}$ the 50 nm film indented by the blunt tip.

6.2 Determination of reduced elastic modulus from pop-in data

In this section the reduced elastic modulus is calculated applying Eqn. (3) on the pop-in data of the 300 nm sample obtained with the blunt and sharp tip. The part of the P- δ curve before the first pop-in event occurs corresponds to purely elastic loading [9], which is described by the Hertzian contact for two elastic solids

$$P = \frac{4}{3}E^*R^{\frac{1}{2}}h_t^{\frac{3}{2}} \quad (14)$$

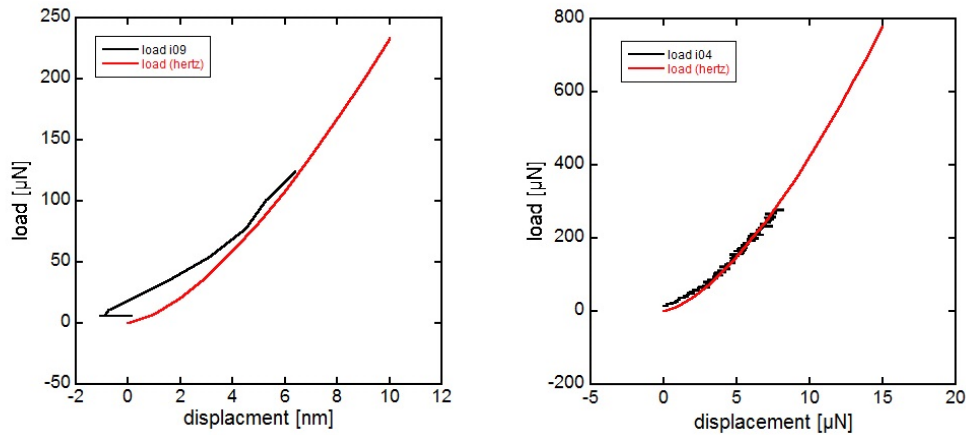
where P is the indentation load, E^* the reduced elastic modulus, R the tip radius and h_t the displacement.

The idea behind this calculation shall be explained as follows: the 300 nm single crystal Cu film is thick enough to have several pop-ins, which makes it possible to apply Eqn. (14) to the elastic loading of this data. Since the tip radii were already calculated in section 4.1, 300 nm and 1.6 μm and are therefore known, Eqn. (14) provides values for the reduced elastic modulus using preassumed values for the load and displacement. Furthermore the correct values for the elastic moduli of sapphire and Cu can be found in literature, which makes it possible to calculate the corresponding reduced moduli from

$$\frac{1}{E^*} = \frac{(1 - \nu_1^2)}{E_1} + \frac{(1 - \nu_2^2)}{E_2} \quad (15)$$

with E_1 and ν_1 being the modulus and Poisson's ratio of the sample and E_2 and ν_2 the respective values of the indenter. For Cu this provides a value of 109.4 GPa and for sapphire 329 GPa. The idea was to investigate if by fitting the calculated values for the reduced moduli, which correspond to the elastic behaviour only, to the elastic loading part of the data, this would render a proper reduced elastic modulus for the thin film, which would be that of Cu.

The plots obtained from the calculated reduced moduli and fitted to the elastic pop-in data are shown Fig. 37 for the blunt and the sharp tip.



(a) Fitting the Hertzian loading for calculated $E^*=320$ GPa and the sharp tip to pop-in data. (b) Fitting the Hertzian loading for calculated $E^*=140$ GPa and tip berk to pop-in data.

Figure 37: Suitable fit between the experimental pop-in data and the Hertzian elastic contact.

All assessed values are found in Tab. 7. The entirety of all reduced moduli leads to a margin of deviation graphically depicted in Fig. 38. It is evident from Tab. 7 that the reduced modulus obtained with the sharp tip is closer to the bulk reduced modulus of sapphire, with an influence of 86 % from the substrate. The reduced modulus obtained with the blunt tip is more influenced by the thin film, with a contribution of 55 % from the coating. This arises a discrepancy since only pop-in data was used, which corresponds to pure elastic loading and with excursion events below displacements of 30 nm, hence below 10 % of the film thickness and therefore should remain uninfluenced by the substrate if the 10 % rule of thumb were to apply to the elastic modulus. Yet the difference in measurement for the tip sizes is large, clearly showing a preference towards substrate values for the sharp tip. If the 10 % rule of thumb were valid for the estimation of reduced elastic modulus, such a strong tendency towards bulk substrate values should not occur. It can therefore not be suggested that the 10 % rule of thumb works for the extraction of reduced elastic modulus for thin films.

Table 7: Hertzian fit of reduced elastic modulus E^*

E^* 300 nm [GPa] sharp tip	E^* 300 nm [GPa] blunt tip
300	260
320	170
280	140
270	210
300	230
290	230
330	220
298.57 +/- 21.15	208.57 +/- 40.6

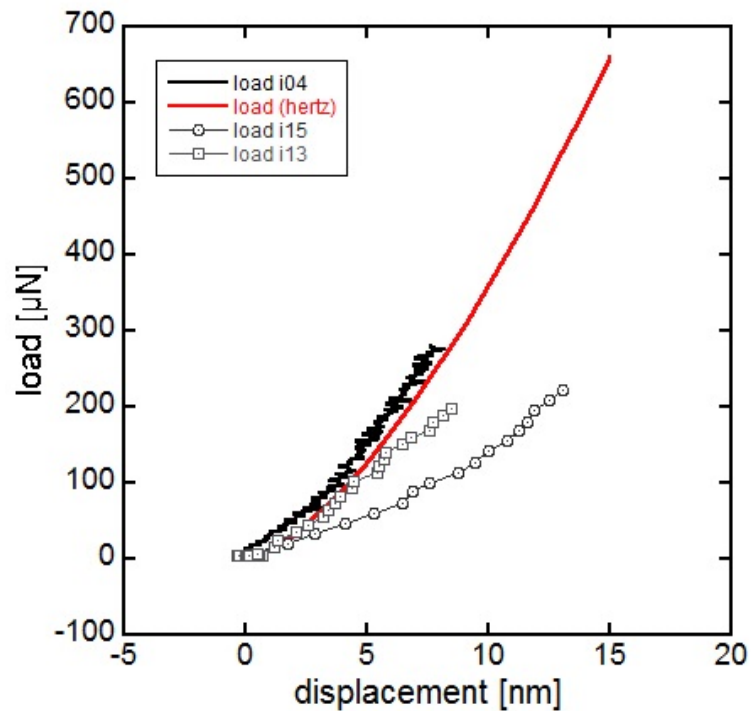


Figure 38: Hertzian loading for different E^* with fitting to pop-in data.

6.3 Plastic and Elastic Zones

In this section it shall be investigated why hardness could be suitably estimated and why elastic modulus failed to provide reliable results for a thin film. Perhaps the main difference between the two material properties is

that hardness is calculated from plastic deformation and elastic modulus is related to the elastic response of a material.

Tabor [24] stated that hardness is intrinsically dependent on plastic deformation only. When the indenter is applied with a load, a plastic zone starts to build underneath it. The size of this zone can be calculated from

$$c = \left[\frac{3P}{2\pi\sigma_{ys}} \right]^{\frac{1}{2}} \quad (16)$$

and the results are listed in Tab. 8 and 9 for the sharp and blunt tip. The zone size was only considered for shallow indentation depths as the zone would outgrow the film thickness with increasing indentation load. When this zone can fully form and is not confined by the substrate, hardness should be measured unrestricted. The plastic zone size easily outgrew the 50 nm and 100 nm film thickness but remains within the 300 nm thickness.

Tabor [24] stated from former research that the estimation of the indentation modulus is influenced by the hydrostatic pressure. Mook and Gerberich [26] investigated this influence especially on sapphire. The region of influence of the hydrostatic pressure is said to be three times the plastic zone size, thus being far larger the film thickness. Stresses are stored elastically within this region as long as the contact is sustained and contribute to the measurement of the reduced elastic modulus. Upon load removal no permanent deformation is visible. In this thesis there were several problems with estimating the reduced elastic modulus, which can likely be related to the extent of the elastic region, which reaches far into the substrate and thus hinders the correct measurement of reduced modulus. The condition is illustrated in Fig. 39.

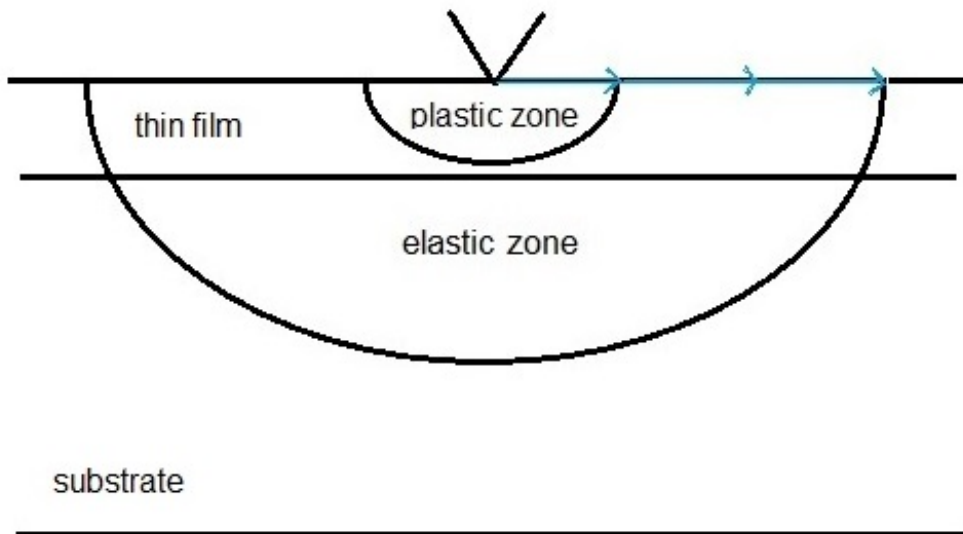


Figure 39: Graphic depiction of the elastic and plastic zone sizes.

Table 8: List of plastic zone sizes for the sharp tip

sample	plastic zone radius [nm]
50 nm	194-212
100 nm	203-269
300 nm	106-358
bulk Cu	152-172
bulk sapphire	132-260

Table 9: List of plastic zone sizes for the blunt tip

sample	plastic zone radius [μm]
50 nm	183-295
100 nm	247-285
300 nm	180-388
bulk Cu	357-578
bulk sapphire	351-552

As observed in Tab. 8 and 9, the plastic zone sizes are larger for the blunt tip, whereas the sharp tip yields a smaller plastic zone radius. This condition seems physically correct since larger indenter areas lead to a broader distributed stress field. The plastic zone radii are larger than the film thicknesses with exception for the 300 nm film. This leads to a discrepancy as for small indentation depths artifacts affect the measurement and lead to increased hardness values even though the plastic zone size is confined within the film thickness. Even though the plastic zone size is larger than the film thickness it is not exceedingly larger than the 100 nm and 50 nm thin film and thus could positively affect the determination of hardness. The bulk values are indifferent to the plastic zone size because no substrate prohibits its formation.

7 Conclusions

A thorough investigation of single crystal thin film behaviour with respect to varying film thicknesses and tip sizes has been undertaken. The $P-\delta$ curves provide general insight whether the deformation of a sample system is more elastic or plastic, if the penetrations reach past the interface, the tip size effects on obtained $P-\delta$ curves and if pop-ins occur.

The focus of this thesis mainly was the determination of hardness and modulus. The suggestion that hardness can be well estimated within and even past 10 % of the film thickness for films at least 300 nm thick is supported. It was observed that hardness scales with decreasing film thickness, similar to the Hall-Patch law for fine grained microstructures. This is consistent with the findings of other studies [30]. Hardness was corrected for pile-up implementing the actual contact area to the determination. It was confirmed that hardness is overestimated by the Oliver-Pharr method. Since pile-up occurs with many different materials, there is a strong demand to incorporate a correction for this measurement artifact in the testing procedure.

In terms of pop-ins it was found that a blunt tip generates slightly more yield excursions as a sharp tip would. The yield instabilities of thin films were shorter than the bulk pop-ins. This was attributed to the constraint of the substrate hindering material flow and the dislocation density.

The determination of elastic modulus using the Oliver-Pharr method did not provide suitable results. The scatter and deviation from literature values were large. Estimating the reduced elastic modulus from pop-in data did not improve the outcome. It is believed that the hydrostatic pressure needs to be accounted for. In usual procedures this is not the case, thus rendering it impossible to estimate modulus correctly for films less than 300 nm thick. It is necessary to investigate the impact of hydrostatic pressure on the extraction of reduced modulus. Since the elastic zone size is three times that of the plastic, there is particular demand for larger film thicknesses, likely

in the range of 1 μm . This arises the question whether such thin films can be fabricated using MBE and requires further research. For thinner films the reduced elastic modulus might still be estimated correctly, as long as substrate and film have similar elastic moduli. The continuous stiffness method [33] is regarded to deliver appropriate values in this case, but was not investigated.

Nanoindentation remains a powerful tool to examine mechanical properties at very small scales. The variety of substrate-film systems to be probed is ever expanding and so is the outcome of their testing. Although a great effort has already been made to provide a proper testing procedure that works well for bulk materials and thin films, it remains a great challenge to reduce the spectrum of mechanical properties and dimensional scales of materials to a common denominator.

References

- [1] T.-H. Fang, S.-R. Jian, and D.-S. Chuu, “Nanomechanical properties of lead zirconate titanate thin films by nanoindentation,” *Journal of Physics: Condensed Matter*, vol. 15, no. 30, p. 5253, 2003.
- [2] T.-H. Fang, W.-J. Chang, and C.-M. Lin, “Nanoindentation characterization of zno thin films,” *Materials Science and Engineering: A*, vol. 452, pp. 715–720, 2007.
- [3] H. Li and J. J. Vlassak, “Determining the elastic modulus and hardness of an ultra-thin film on a substrate using nanoindentation,” *Journal of Materials Research*, vol. 24, no. 3, pp. 1114–1126, 2009.
- [4] G. Pharr and W. Oliver, “Measurement of thin film mechanical properties using nanoindentation,” *Mrs Bulletin*, vol. 17, no. 7, pp. 28–33, 1992.
- [5] T. Tsui and G. Pharr, “Substrate effects on nanoindentation mechanical property measurement of soft films on hard substrates,” *Journal of Materials Research*, vol. 14, no. 1, pp. 292–301, 1999.
- [6] R. Saha and W. D. Nix, “Effects of the substrate on the determination of thin film mechanical properties by nanoindentation,” *Acta materialia*, vol. 50, no. 1, pp. 23–38, 2002.
- [7] W. D. Nix and H. Gao, “Indentation size effects in crystalline materials: a law for strain gradient plasticity,” *Journal of the Mechanics and Physics of Solids*, vol. 46, no. 3, pp. 411–425, 1998.
- [8] H. Buckle, J. Westbrook, and H. Conrad, “The science of hardness testing and its research applications,” *American Society for Metals*, vol. 453, 1973.
- [9] S.-H. Hong, K. Kim, Y.-M. Kim, J.-H. Hahn, C.-S. Lee, and J.-H. Park, “Characterization of elastic moduli of cu thin films using nanoindentation,”

- tion technique,” *Composites science and technology*, vol. 65, no. 9, pp. 1401–1408, 2005.
- [10] J. Menčík, D. Munz, E. Quandt, E. Weppelmann, and M. Swain, “Determination of elastic modulus of thin layers using nanoindentation,” *Journal of Materials Research*, vol. 12, no. 9, pp. 2475–2484, 1997.
- [11] M. Cordill, D. Hallman, N. Moody, D. Adams, and W. W. Gerberich, “Thickness effects on the plasticity of gold films,” *Metallurgical and Materials Transactions A*, vol. 38, no. 13, pp. 2154–2159, 2007.
- [12] A. A. Volinsky, N. R. Moody, and W. W. Gerberich, “Nanoindentation of au and pt/cu thin films at elevated temperatures,” *Journal of Materials Research*, vol. 19, no. 9, pp. 2650–2657, 2004.
- [13] J. Hay, “Introduction to instrumented indentation testing,” *Experimental techniques*, vol. 33, no. 6, pp. 66–72, 2009.
- [14] A. Kleinbichler, J. Zechner, and M. Cordill, “Buckle induced delamination techniques to measure the adhesion of metal dielectric interfaces,” *Microelectronic Engineering*, vol. 167, pp. 63–68, 2017.
- [15] B. R. Lawn, A. Evans, and D. Marshall, “Elastic/plastic indentation damage in ceramics: the median/radial crack system,” *Journal of the American Ceramic Society*, vol. 63, no. 9-10, pp. 574–581, 1980.
- [16] A. Fischer-Cripps and D. Nicholson, “Nanoindentation. mechanical engineering series,” 2004.
- [17] T. Page and S. Bull, “Measuring and modelling the instrumented indentation (nanoindentation) response of coated systems,” *Philosophical Magazine*, vol. 86, no. 33-35, pp. 5331–5346, 2006.
- [18] M. J. Cordill, N. R. Moody, and W. W. Gerberich, “Size effects on yield instabilities in nickel,” *MRS Online Proceedings Library Archive*, vol. 976, 2006.

- [19] S. Suresh, T.-G. Nieh, and B. Choi, "Nano-indentation of copper thin films on silicon substrates," *Scripta Materialia*, vol. 41, no. 9, pp. 951–957, 1999.
- [20] M. Cordill, N. Moody, and W. W. Gerberich, "The role of dislocation walls for nanoindentation to shallow depths," *International Journal of Plasticity*, vol. 25, no. 2, pp. 281–301, 2009.
- [21] N. Moharrami and S. Bull, "A comparison of nanoindentation pile-up in bulk materials and thin films," *Thin Solid Films*, vol. 572, pp. 189–199, 2014.
- [22] R. Saha and W. Nix, "Soft films on hard substrates—nanoindentation of tungsten films on sapphire substrates," *Materials Science and Engineering: A*, vol. 319, pp. 898–901, 2001.
- [23] D. Kramer, H. Huang, M. Kriese, J. Robach, J. Nelson, A. Wright, D. Bahr, and W. W. Gerberich, "Yield strength predictions from the plastic zone around nanocontacts," *Acta Materialia*, vol. 47, no. 1, pp. 333–343, 1998.
- [24] D. Tabor, "The physical meaning of indentation and scratch hardness," *British Journal of Applied Physics*, vol. 7, no. 5, p. 159, 1956.
- [25] W. D. Callister, D. G. Rethwisch *et al.*, *Materials science and engineering: an introduction*. John wiley & sons New York, 2007, vol. 7.
- [26] W. M. Mook and W. Gerberich, "Effect of hydrostatic pressure on indentation modulus," *MRS Online Proceedings Library Archive*, vol. 1049, 2007.
- [27] E. Hall, "The deformation and ageing of mild steel: Iii discussion of results," *Proceedings of the Physical Society. Section B*, vol. 64, no. 9, p. 747, 1951.
- [28] N. Petch, "The cleavage strength of polycrystals," *Journal of the Iron and Steel Institute*, vol. 174, pp. 25–28, 1953.

- [29] W. D. Nix, "Elastic and plastic properties of thin films on substrates: nanoindentation techniques," *Materials Science and Engineering: A*, vol. 234, pp. 37–44, 1997.
- [30] S. Soare, S. Bull, A. O'Neil, N. Wright, A. Horsfall, and J. dos Santos, "Nanoindentation assessment of aluminium metallisation; the effect of creep and pile-up," *Surface and Coatings Technology*, vol. 177, pp. 497–503, 2004.
- [31] A. Kelly and K. M. Knowles, *Crystallography and crystal defects*. John Wiley & Sons, 2012.
- [32] D. Dorset, "X-ray diffraction: a practical approach," *Microscopy and microanalysis*, vol. 4, no. 5, pp. 513–515, 1998.
- [33] T. Page, G. Pharr, J. Hay, W. Oliver, B. Lucas, E. Herbert, and L. Riester, "Nanoindentation characterisation of coated systems: P: S 2-a new approach using the continuous stiffness technique," *MRS Online Proceedings Library Archive*, vol. 522, 1998.